Mechanical Analysis for New and Spent Fuel Storage Racks

Revision 0

Non-Proprietary

December 2014

REVISION HISTORY

Revision	Date	Page	Description
0	December 2014	All	First Issue

ABSTRACT

This report shows the structural integrity of the new and the spent fuel storage racks under operating conditions including the postulated loading conditions for the APR1400 design. All analyses and evaluations are performed based on the NRC standard review plan 3.8.4, appendix D.

This report includes the design and geometry features, structural and seismic analysis, and mechanical accident analysis of the new and the spent fuel storage racks for the APR1400 design.

The nonlinear dynamic analysis for the new and the spent fuel storage racks under operating conditions is performed using a single or a whole pool multi-rack analysis model with time-history seismic loads. The loads and the displacements by dynamic simulations are calculated to demonstrate the structural integrity of the new and the spent fuel storage racks. Overturning of rack is evaluated by showing that the rack does not exhibit a rotation sufficient to bring the center of mass over the corner pedestal. The lateral impact load on the spent fuel assembly is evaluated for two acceptance criteria; fuel spacer grid bucking and fuel rod cladding yield stress. All stress evaluations for the fuel racks are performed based on the worst-case results from dynamic simulations in accordance with ASME Code Section III, Division 1, Subsection NF requirements for Class 3 component supports.

The mechanical accidents analyses are performed based on four scenarios; drops of the fuel assembly along with the handling tool on a top edge of the rack, an interior cell away from the support pedestals, or the cell located above a support pedestal, and the stuck fuel assembly. For the drop accidents, the deformations of the cell wall and the baseplate are calculated by using the energy balance equation between the kinetic energy by the impact and the energy dissipated by plastic deformation. This will ensure that the configuration analyzed in the criticality evaluation remains valid and the deformed baseplate of the rack does not impact the pool liner. For the postulated stuck fuel uplift event, the structural integrity of the spent fuel storage racks is evaluated by using the classical strength of materials equation. This analysis is performed to demonstrate that the damage of the cell wall is limited to the portion of the rack structure above the neutron absorber.

As results of the structural and seismic analysis, it is concluded as follows: (1) there is no impact of the rack-to-pool wall and on the rack cell-to-cell; (2) overturning of the racks does not occur; (3) the fuel spacer grid does not buckle and the bending stress induced in the fuel rod cladding is well below the yield strength of the fuel rod clad; and (4) the calculated stresses on the racks are below the allowable stress limits of the ASME Boiler and Pressure Vessel Code Section III, Division 1, Subsection NF requirements for Class 3 component supports.

As results of the mechanical accident analysis, it is concluded as follows: (1) there is no effect on the sub-criticality of the fuel in adjacent cells due to a mechanical drop accident; (2) the baseplate does not experience puncture and the downward displacement of the baseplate will not lead to a secondary impact of the dropping mass with the pool liner; (3) a stuck fuel assembly does not cause a bounding stress condition.

Therefore, the new and the spent fuel storage racks for the APR1400 design meet the requirements of the NRC standard review plan 3.8.4, appendix D.

TABLE OF CONTENTS

ABSTRACT iii
LIST OF TABLES vi
LIST OF FIGURES vii
ACRONYMS AND ABBREVIATIONS viii
1 INTRODUCTION 1
2 FUEL RACKS 2
2.1 Description of New Fuel Storage Racks 2
2.2 Description of Spent Fuel Storage Racks 2
3 STRUCTURAL AND SEISMIC ANALYSIS 11
3.1 Methodology 11
3.1.1 Acceleration Time Histories Generation 11
3.1.2 Modeling 11
3.1.3 Simulation and Solution Methodology 15
3.2 Acceptance Criteria 15
3.2.1 Kinematic Criteria 15
3.2.2 Stress Limit Criteria 15
3.2.3 Dimensionless Stress Factors 18
3.3 Assumptions 18
3.4 Input Data 18
3.4.1 Rack Data 18
3.4.2 Fuel Assembly Data 18
3.4.3 Structural Damping 18
3.4.4 Material Data 19
3.5 Computer Codes 19
3.6 Dynamic Simulations 19
3.7 Results of Analyses 19
3.7.1 Time History Simulation Results 19
3.7.2 Fuel Structural Evaluation 20
3.7.3 Rack Structural Evaluation 22
4 MECHANICAL ACCIDENTS ANALYSIS 38
4.1 Description of Mechanical Accidents 38
4.2 Acceptance Criteria 38
4.3 Analysis Method 39

4.3.1 Calculation of Impact Velocity 39
4.3.2 Methodology for Straight Shallow Drop Accident 40
4.3.3 Methodology for Straight Deep Drop Accident (Away from the Pedestal) 41
4.3.4 Methodology for Straight Deep Drop Accident (Over a Pedestal) 42
4.3.5 Methodology for Stuck Fuel Accident 42
4.4 Assumptions 43
4.5 Results of Analyses 43
5 CONCLUSIONS 49
6 REFERENCES 50

LIST OF TABLES

Table 2-1 Dimensions Data of NFSR 3
Table 2-2 Dimensions Data of SFSR 4
Table 3-1 Load Combinations for Rack Analysis 26
Table 3-2 Rack Size and Weight 27
Table 3-3 Data of Fuel Assembly 28
Table 3-4 Material Properties 28
Table 3-5 Computer Codes used in Mechanical Analysis 29
Table 3-6 List of Simulation 29
Table 3-7 Displacement of Racks 30
Table 3-8 Maximum Loads on Rack Module 31
Table 3-9 Maximum Loads on Single Pedestal 31
Table 3-10 Impact Loads on Rack 32
Table 3-11 Stress Evaluation for Fuel Assembly 32
Table 3-12 Maximum Stress Factors of Rack 33
Table 3-13 Stress Evaluation for Fuel Racks 33
Table 4-1 Impact Evaluation Data 45

LIST OF FIGURES

Figure 2-1 Layout and Plan View of NFSR 5
Figure 2-2 Isometric Schematic of NFSR 6
Figure 2-3 Layout of SFSR 7
Figure 2-4 Plan View of SFSR 8
Figure 2-5 Isometric Schematic of SFSR (Region I) 9
Figure 2-6 Isometric Schematic of SFSR (Region II) 10
Figure 3-1 Dynamic Analysis Model of NFSR 34
Figure 3-2 Dynamic Analysis Model for Whole Pool Multi-Rack 35
Figure 3-3 Dynamic Analysis Model of SFSR 36
Figure 3-4 Schematic of Spring Elements used for SFSR 37
Figure 4-1 Schematic of the Straight Shallow Drop 46
Figure 4-2 Schematic of the Deep Drop Scenario-1 47
Figure 4-3 Schematic of the Deep Drop Scenario-2 48

ACRONYMS AND ABBREVIATIONS

ASME	American Society of Mechanical Engineers
B&W	Babcock and Wilcox
COF	coefficient of friction
E-W	east-west
KEPCO	Korea Electric Power Corporation
KHNP	Korea Hydro & Nuclear Power Co., Ltd.
NFP	new fuel pool
NFSR	new fuel storage rack
N-S	north-south
NRC	U.S. Nuclear Regulatory Commission
OBE	operating basis earthquake
PSD	power spectra density
PWR	pressurized water reactor
RG	regulatory guide
SFP	spent fuel pool
SFSR	spent fuel storage rack
SRP	standard review plan
SRSS	square root of the sum of the squares
SSE	safe shutdown earthquake
WPMR	whole pool multi-rack

1 INTRODUCTION

This report is prepared to show the structural adequacy of the new fuel storage racks (NFSRs) and the spent fuel storage racks (SFSRs) under operating conditions including the postulated loading conditions for the APR1400 design. All analyses are performed based on the U.S. Nuclear Regulatory Commission (NRC) standard review plan (SRP) 3.8.4, appendix D (Reference 1).

Section 2 describes the design and geometry features of the NFSRs and the SFSRs for the APR1400 design. Section 3 includes the analysis methods, acceptance criteria, modeling assumptions, significant results of dynamic simulations, and stress evaluations for a seismic loading. Section 4 presents the methodology, assumptions, and significant results of mechanical accidents analyses.

2 FUEL RACKS

2.1 Description of New Fuel Storage Racks

Figure 2-1 shows the storage layout and the plan view of the two 7 x 8 cells modules of the NFSR in the new fuel pool (NFP) of the APR1400 design. The rack modules are designed as cellular structures which are supported by top, middle, base plates and x-plates. There is a little gap between the fuel assembly and the walls of the cell in the NFSRs. The NFSRs are installed in a dry new fuel pool. These racks are held down by firmly attached to the embedment plates of NFP using a stud bolt. Therefore, there is no possibility of overturning for the NFSR. The new fuel storage racks provide onsite storage capacity of 112 new fuel assemblies corresponding to one refueling batch plus additional margin. The center-to-center spacing between adjacent fuel assemblies is 35.5 cm (14 in) to maintain subcriticality. The cell wall thickness of the NFSR is 6 mm (0.236 in). The principal construction materials for the NFSRs are SA-240 Type 304L for cells and plates, and SA-564 Grade 630 for support stud, respectively. In addition, the NFSR is designed without using the neutron absorber material (METAMIC^{TM}). Figure 2-2 shows the isometric schematic of the NFSR. The basic dimensions of the NFSRs are summarized in Table 2-1.

2.2 Description of Spent Fuel Storage Racks

Figures 2-3 shows the storage layout of the SFSRs in the spent fuel pool (SFP) of the APR1400 design. The spent fuel pool is made up of Region I and Region II. The fresh or spent fuel assemblies including damaged fuel assemblies are stored in Region I, which has a storage capacity for one full core, one refueling batch, and five damaged fuels. Region I consists of four 8 x 8 cell modules, which are designated Modules A1-1, A1-2, A1-3 and A1-4, and two 6 x 8 cell modules, which are designated Module A2-1, including the cells for five(5) damaged fuel canisters, and Module A2-2. Region II consists of nineteen 8 x 8 cell modules, which are designated Modules B1, B2-1, B2-2, B2-3, B3, B4, B5-1, B5-2, B5-3, B5-4, B5-5, B5-6, B6-1, B6-2, B6-3, B7, B8, B9 and B10, and four 8 x 7 cell modules, which are designated Modules C1, C2, C3 and C4. Figure 2-4 shows the very tight rack-to-rack and rack-to-wall gaps. The SFSRs described above are free-standing with pedestals resting on embedment plates, which distribute the dead weight of the loaded racks into the reinforced concrete structure of the floor. Each SFSR is supported by four pedestals, which are remotely adjustable. The SFSRs are submerged in water. There is a little gap between the spent fuel assembly and the walls of the cell. Therefore, the motions of racks and the fuel assemblies will be influenced by a fluid-structure interaction.

SFSRs are capable of receiving 1,792 cells and the center-to-center spacing between adjacent fuel assemblies is 27.5 cm (10.83 in) for Region I racks and 22.5 cm (8.86 in) for Region II racks to maintain subcriticality. The cell wall thickness of the SFSRs is 2.5 mm (0.1 in). The principal construction materials for the SFSRs are SA-240 Type 304L for cells and plates, SA-564 Grade 630 for a support stud, and hot-rolled composite plate material (METAMIC^{TM}) for a neutron absorber.

Figures 2-5 and 2-6 show the representative isometric schematics of the Region I and Region II racks, respectively. The basic dimensions of the SFSRs are summarized in Table 2-2.

Table 2-1 Dimensions Data of NFSR

No.	Description	Dimensions(*), mm (in)
1	Cell Length	4,570 (179.9)
2	Cell Thickness	6.0 (0.236)
3	Cell Inside Dimension(Width)	220.0 (8.66)
4	Cell Center-to-Center Pitch	355 (13.98)
5	Baseplate Thickness	25.0 (0.984)
6	Baseplate Flow Hole Diameter	133.0 (5.24)
7	Distance from Baseplate to Liner	210.0 (8.27)
8	Male Pedestal Diameter	90.0 (3.54)

(*) All of the dimensions are nominal values.

Table 2-2 Dimensions Data of SFSR

No.	Description		Dimensions(*), mm (in)
1	Cell Height from Baseplate Top to Rack Top		4,590 (180.7)
2	Cell Thickness		2.5 (0.098)
3	Cell Inside Dimension(Width)		220.0 (8.66)
4	Damaged Fuel Canister Inside Dimension		242.0 (9.53)
5	Cell Pitch	Region I	275.0 (10.83)
		Region II	225.0 (8.858)
6	Baseplate Thickness		25.0 (0.984)
7	Baseplate Hole Diameter		133.0 (5.24)
8	Distance from Baseplate to Liner		185.0 (7.28)
9	Male Pedestal Dia.		90.0 (3.54)
10	Neutron Absorber Material		METAMIC™
11	Neutron Absorber Length		[ ] TS
12	Neutron Absorber Width		[ ]
13	Neutron Absorber Thickness		[ ]
14	Neutron Absorber Sheathing Thickness	Inside	[ ]
		Outside	[ ]
15	Distance from Top of Rack Baseplate to Bottom of Neutron Absorber		[ ]

(*) All of the dimensions are nominal values.

TS

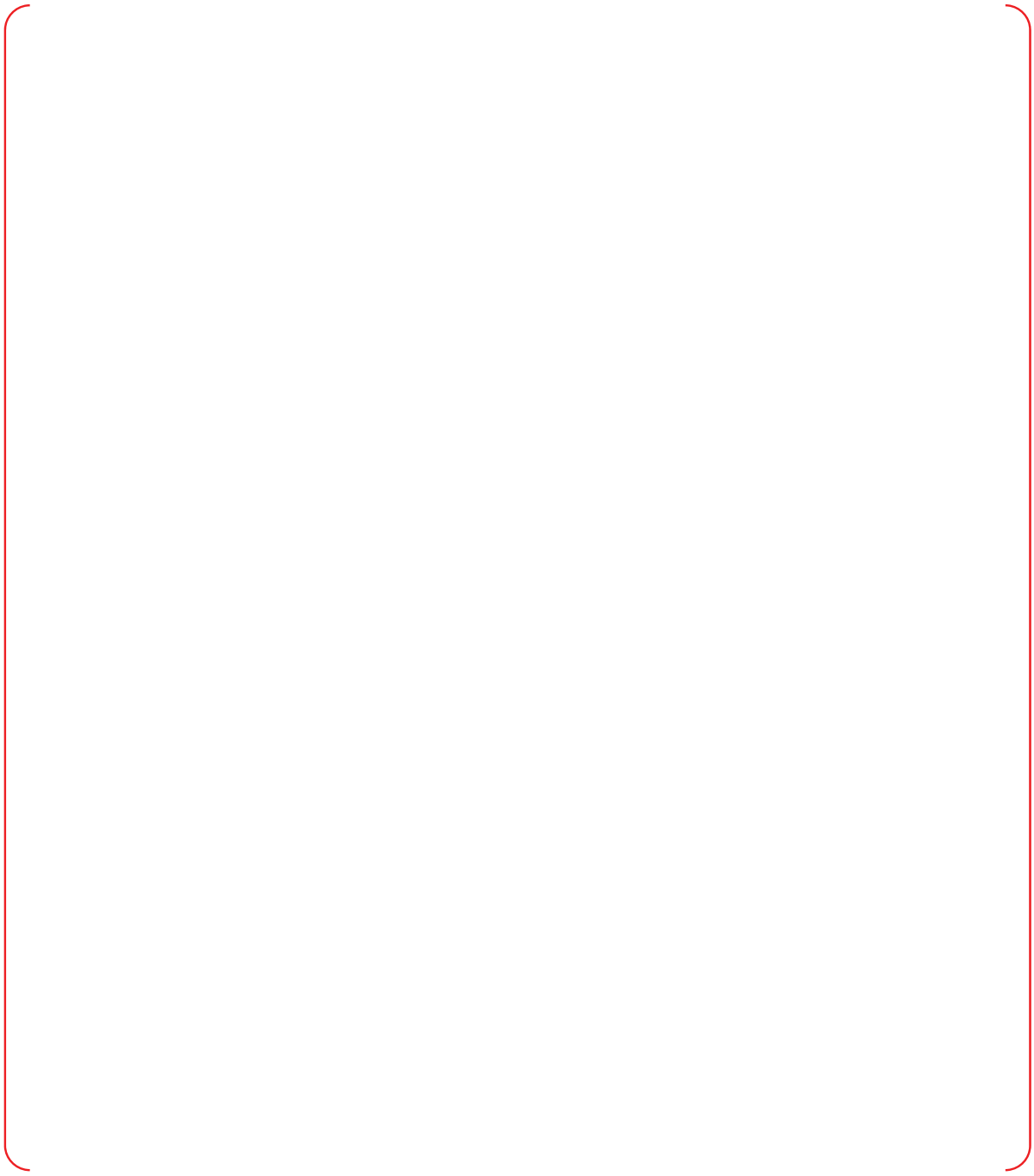

Figure 2-1 Layout and Plan View of NFSR

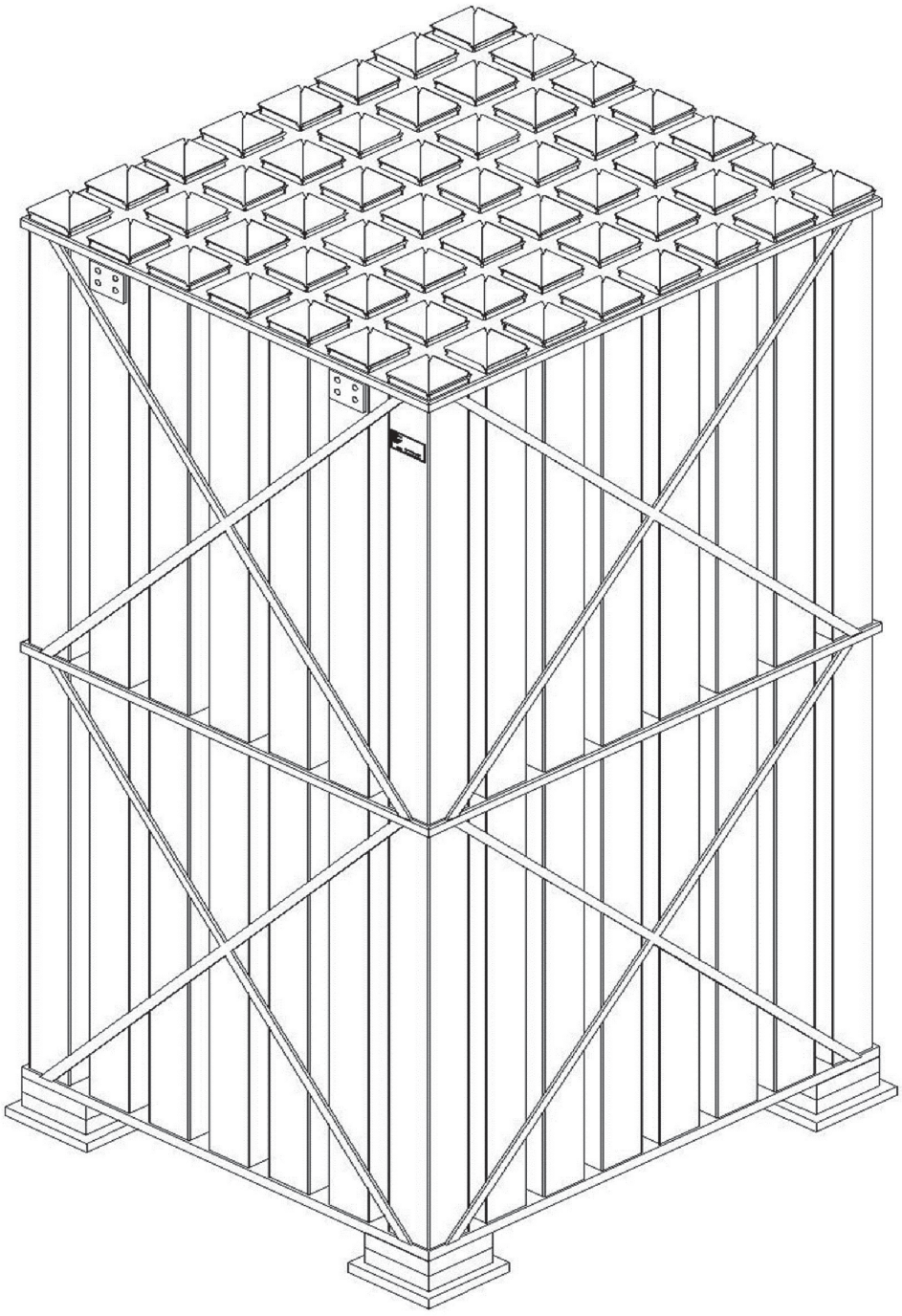

Figure 2-2 Isometric Schematic of NFSR

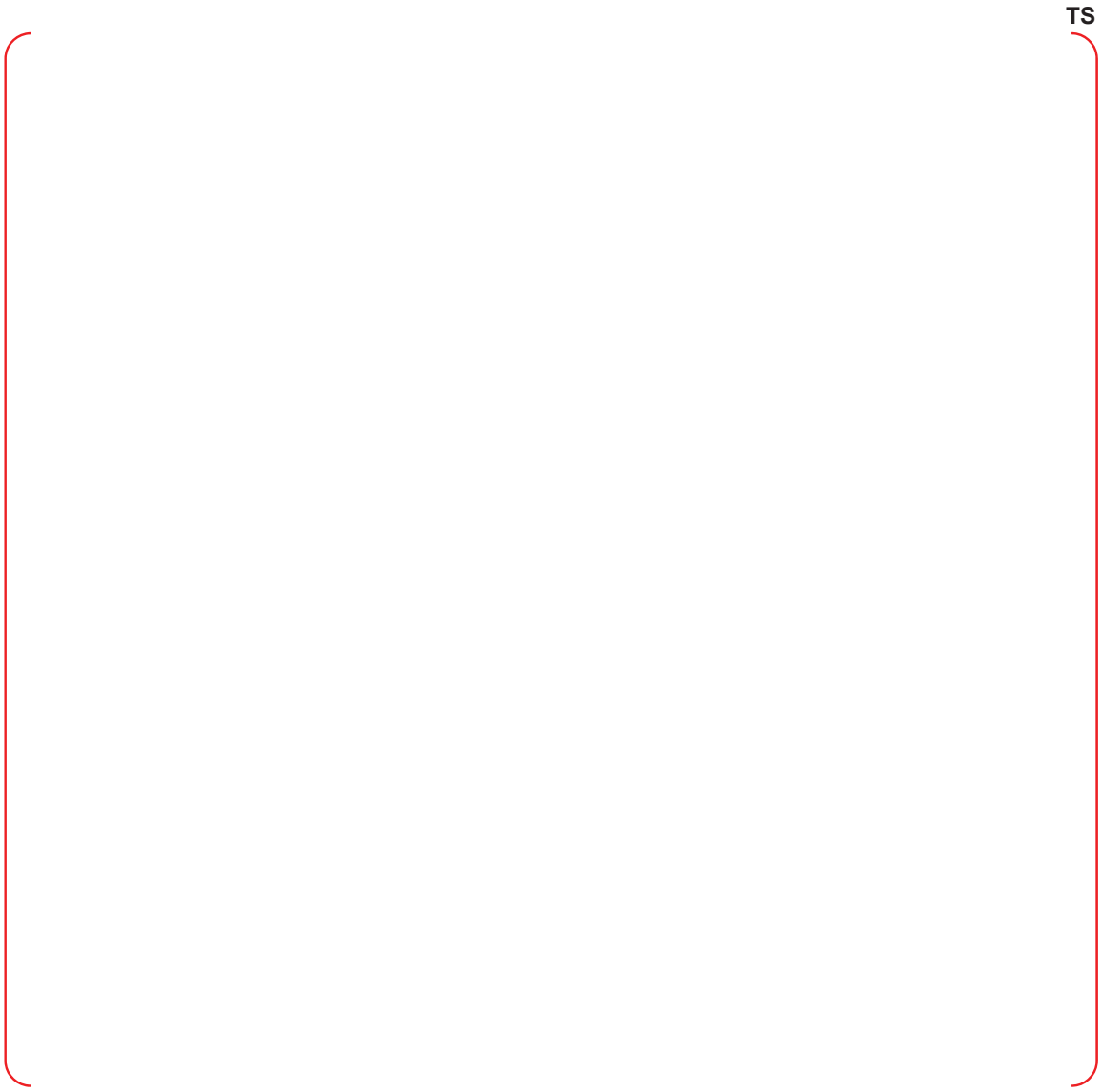

Figure 2-3 Layout of SFSR

TS

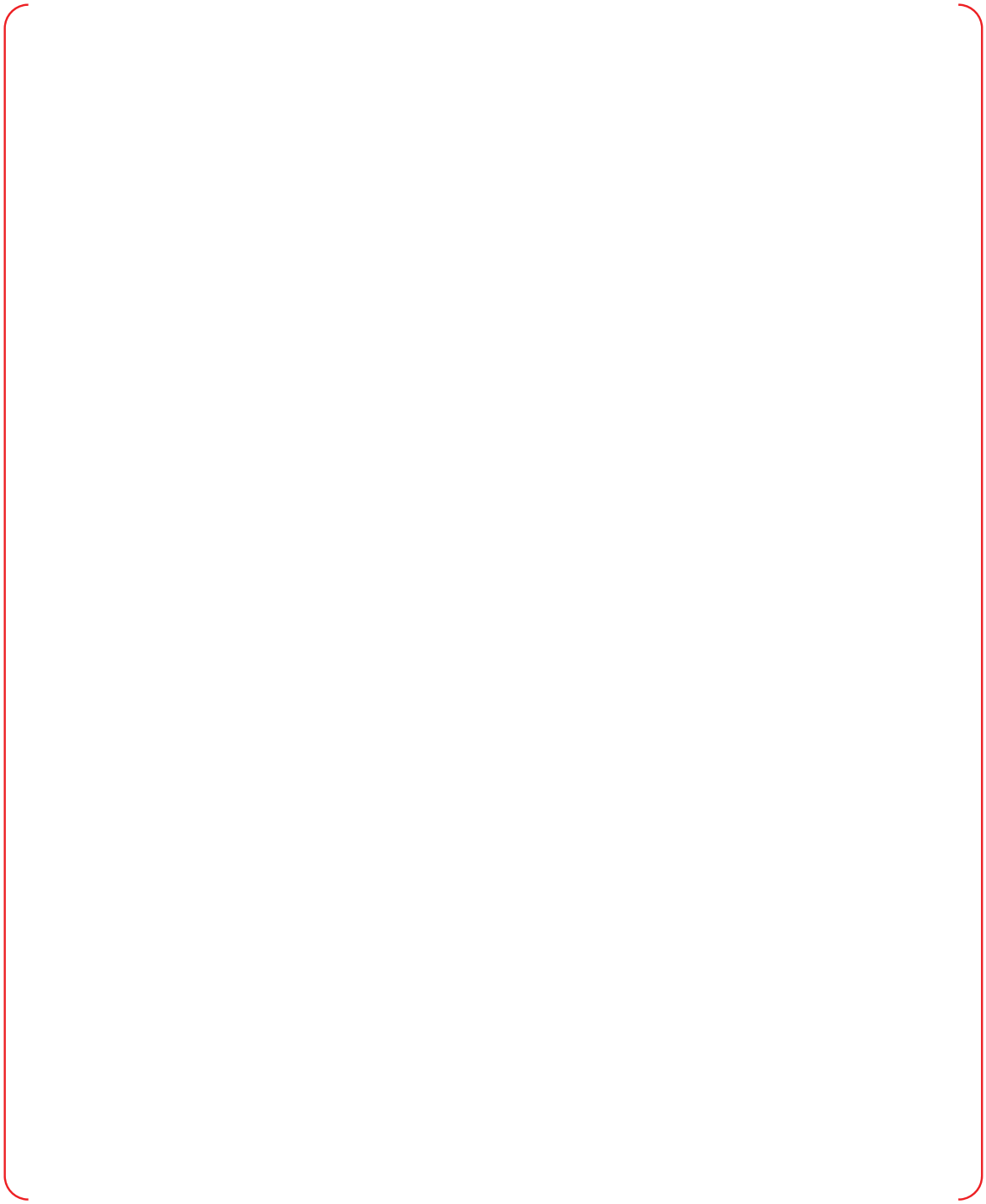

Figure 2-4 Plan View of SFSR

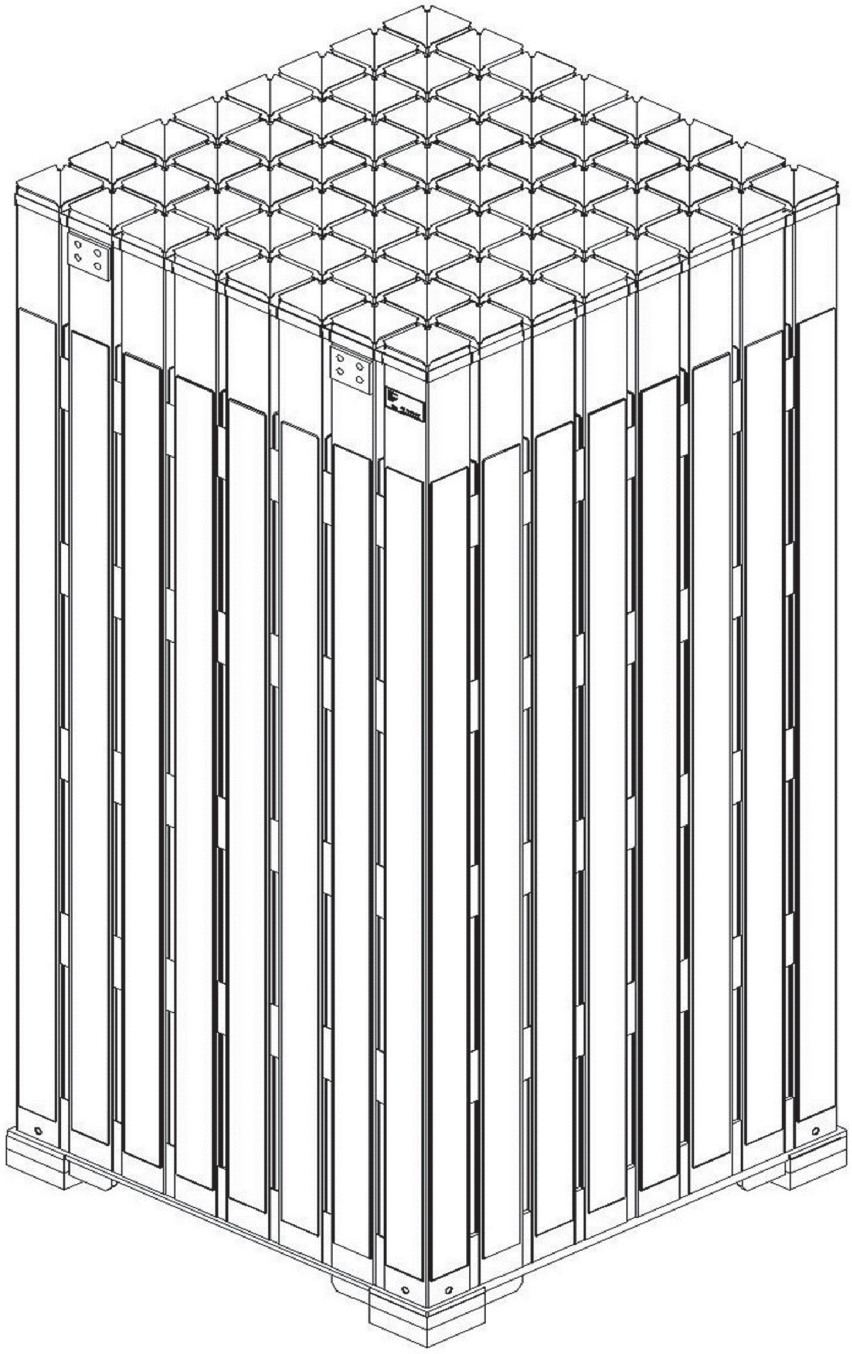

Figure 2-5 Isometric Schematic of SFSR (Region I)

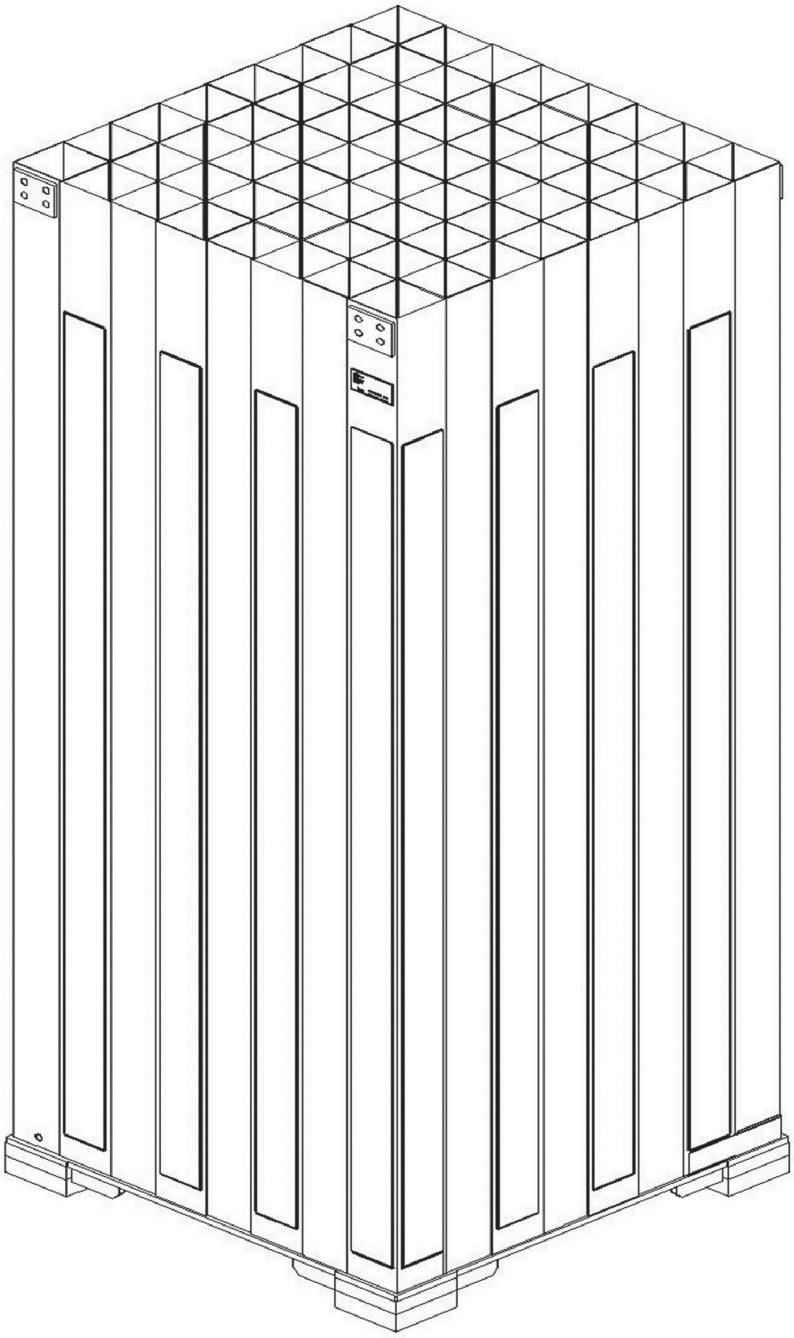

Figure 2-6 Isometric Schematic of SFSR (Region II)

3 STRUCTURAL AND SEISMIC ANALYSIS

The structural and seismic analysis for the NFSRs and the SFSRs includes a dynamic analysis method, modeling details, acceptance criteria for kinematic and stress analysis, assumptions, input data for racks and fuel assembly and significant results of dynamic simulations under seismic loading.

3.1 Methodology

The composite dynamic simulation wherein all racks in the pool are modeled is used to determine the loads and displacements for each fuel storage rack in the pool and the relative motion between racks, and to evaluate the potential damage and consequences of inter-rack and rack-wall impact phenomena in the racks.

3.1.1 Acceleration Time Histories Generation

The response of a free-standing rack module to seismic inputs is highly nonlinear and involves a complex combination of motions such as sliding, rocking, twisting, and turning by impacts and friction effects. Linear methods, such as response spectrum analysis, cannot accurately simulate the structural response of such a highly nonlinear structure to seismic excitation. An accurate evaluation of nonlinear response requires a 3-D time-history analysis to establish the proper response during a seismic loading.

Therefore, the initial step in a 3-D time-history analysis is to develop time-history seismic loadings for three orthogonal directions that comply with the guidelines of the NRC SRP 3.7.1 (Reference 2). The synthetic time-history seismic loadings must meet the criteria of statistical independence, envelop the target response spectra, and envelop the target power spectral density (PSD) curves. The NFSRs and the SFSRs have been analyzed using acceleration time-history loads of safe shutdown earthquake (SSE) for both NFP and SFP storage locations. The design basis response spectra at elevation 137’-6” and 114’-0” of the APR1400 auxiliary building are applied as the target response spectra for the NFP and SFP, respectively.

3.1.2 Modeling

3.1.2.1 General Considerations

A suitable dynamic model for simulations is required. Reliable assessment of the stress field and kinematic behavior of the rack modules calls for a conservative dynamic model incorporating all key attributes of the actual structure. This means that the dynamic model must have the ability to execute concurrent sliding, rocking, bending, twisting, and other motions compatible with free-standing or fixed installation of the modules. Additionally, the model must possess the capability to simulate momentum transfers, which occur due to rattling of fuel assemblies, and lift-off and subsequent impact of support pedestals. The contribution of the water mass in the interstitial spaces around the rack modules and within the storage cells must be considered in an accurate manner.

The model must be able to reflect the friction at the pedestal-to-embedment plate interfaces. The 3-D dynamic analysis model of a typical APR1400 SFSR handles the following parameters.

(1) Coefficient of Friction

Because the spent fuel storage rack is placed but not fixed on pool, sliding can occur between the rack and bottom of pool. Coefficient of friction (COF) values are assigned at each interface, which reflect the realities of wetted stainless steel-to-stainless steel contact in a wet environment. COF may have a rather wide range, depending on the design of those interfaces. The mean value of coefficient of friction is 0.5, and the limiting values are 0.2 and 0.8 which are based on experimental data (Reference 3).

(2) Impact Phenomena

Compression-only spring elements, with gap capability, are used to provide opening and closing of interfaces for the pedestal-to-bearing pad interface, the fuel assembly-to-cell wall interface, and the rack-to-rack and rack-to-pool wall potential contact.

(3) Fuel Loading

The dynamic analyses are performed for the condition that all fuel assemblies are fully loaded in the racks.

(4) Fluid Coupling

If an external load like earthquake occurs, spent fuel storage rack is influenced by fluid movement as well as by mechanical contact because it is submerged in water. This phenomenon is called fluid coupling effect. As the objects adjoin closer to each other, the fluid coupling gives greater effect. Because the racks are densely arranged in the spent fuel pool, the fluid coupling effect strongly acts on adjacent racks by the water of the pool. The formula for a hydrodynamic effect of the adjacent storage racks due to a storage rack in the spent fuel pool (Reference 4) is adopted. This formula is based on the potential flow theory of Fritz (Reference 5) and calculates the values of hydrodynamic mass of two objects in the fluid.

Fritz's classical two-body fluid coupling model (Reference 5) is extended to multiple bodies and used to perform a three-dimensional multi-rack analysis. This technology is incorporated in the whole pool multi-rack (WPMR) analysis, which permits simultaneous simulation of all racks in the pool. In its simplest form, fluid coupling effect can be explained by considering the proximate motion of two bodies (for example, a rack and a wall) under water. If one body (mass M_1) vibrates adjacent to a second body (mass M_2), and both bodies are submerged in frictionless fluid, Newton's equations of motion for the two bodies are as follows:

$-M_H A_1 + (M_1 + M_H) A_2$ = Fluid reaction forces on mass M_1, and
$(M_1 + M_H) A_1 - (M_1 + M_2 + M_H) A_2$ = Fluid reaction forces on mass M_2,

where,

M_1 = Mass of fluid displaced by the inner body,
M_2 = Mass of fluid inside the outer body in the absence of the inner body,
A_1, A_2 = Absolute accelerations of masses M_1 and M_2, respectively, and
M_H = Hydrodynamic mass that depends on the fluid flow when the two bodies move relative to each other.

The fluid adds mass to the body (M_H to mass M_1), and may be considered an inertial force proportional to acceleration of the adjacent body (mass M_2). Thus, acceleration of one body affects the force on another. This force is a function of a gap between bodies. Lateral motion of a fuel assembly inside a storage location is subject to this effect. Generally, the fluid coupling is always present when a series of closely spaced bodies (for example, fuel racks) undergo transient motion in a submerged environment of SFP. Therefore, the kinematics phenomenon of the storage rack in the spent fuel pool is indicated by analysis which includes a hydrodynamic effect. However, the NFSRs have no hydrodynamic effect because it is installed in air.

3.1.2.2 Details for Rack and Fuel Assembly

The dynamic analysis model of new fuel storage rack is shown in the Figure 3-1. Figure 3-2 is whole pool multi-rack analysis model of spent fuel storage rack. It is overall dynamic analysis model of spent fuel storage rack created by combining the model shown in the Figure 3-3 for Region I and Region II.

Figure 3-3 shows the sketch of nodes and elements of a dynamic analysis model for the SFSR. The racks and fuel assemblies are modeled as 3-D elastic beam (BEAM4) and lumped mass (MASS21) of ANSYS finite element analysis program (Reference 6). The BEAM4 element indicates the dynamic characteristics of storage racks using the effective structural property. Effective structural properties for the dynamic model are determined from the natural frequencies and mode shapes of the detailed model. Details of effective structural properties for the APR1400 racks are shown in Reference 7.

There are three nodes for rack cells and fuel assemblies, respectively. Two nodes are located in the baseplate and the upper end of each storage rack, respectively. One node is located in its center. Each node of the elements for racks has a displacement and rotation degree of freedom in each direction and a lumped mass with it. In addition, that for fuel assemblies has a degree of freedom in the horizontal direction. A vertical movement of fuel assembly is assumed to be the same as the vertical movement of the storage racks. The nodes for the rack and the fuel assembly are connected with impact spring elements in the horizontal direction to consider impact by a relative motion of the storage rack and the fuel assembly.

Lumped mass of rack and fuel assemblies is assigned to the three nodes for rack cells and fuel assemblies. All the fuel assemblies in each storage rack module are modeled as one beam of which the mass equals the sum of the masses of all the fuel assemblies in a rack module. Because the fuel assemblies in a rack module are modeled together, all fuel assemblies move simultaneously in one direction. The assumption included in this model brings about larger impact on the rack module than the actual case and results in the conservative loads to the storage rack. The fuel assembly is modeled with only three nodes so that the calculated impact loads on the nodes will be larger than the actual value, because the fuel assembly actually has spacer grids of eleven parts. The mass of the upper, the central and the lower nodes is 1/4, 1/2 and 1/4 of the total mass, respectively.

Figure 3-4 shows a two-dimensional elevation schematic depicting the three masses of fuel and rack cells, and their associated fuel assembly/rack cell spring elements, the support pedestal spring elements, and adjacent rack impact spring elements. Nonlinear gap element and linear friction spring element are used to represent the vertical and horizontal motions of support pedestals, respectively. These elements are used in the representation of slant or sliding phenomenon of the storage rack. A directional stiffness value of pedestals is assigned to linear friction spring element. The pool bottom is assumed as a rigid body, and is contacted with pedestals. In order to represent an impact of rack-to-rack and rack-to-pool wall, compression impact spring elements between the lumped masses are used. Impact spring element of horizontal direction between racks is assigned to upper and lower of storage rack. The initial distance between impacts objects is determined by arrangement of storage rack, size of fuel assembly and cell. Stiffness and masses of racks are different according to size and characteristics.

The hydrodynamic masses on rack-to-fuel, rack-to-rack, and rack-to-pool wall are modeled as mass MATRIX27 element of ANSYS finite element analysis program (Reference 6). This element connects two nodes for the rack-to-fuel, rack-to-rack, and rack-to-pool wall.

3.1.2.3 Hydrodynamic Mass

In addition to the structural mass of racks and fuel assemblies, hydrodynamic masses of rack-to-rack and rack-to-fuel assembly for the SFSRs are included in the total mass to consider the fluid coupling effect. Details for the hydrodynamic mass are described in the followings:

(1) Between Cell and Fuel Assembly

Fuel assembly consists of several fuel rods and guide tubes, and is supported by spacer grid. A hydrodynamic mass is calculated assuming the structure as of long cylinders whose centers match with the center of the structure. A hydrodynamic mass acting at the centers of the two rigid bodies and liquid filled therein is represented using following formula of Reference 4.

$$M_H = \left[\frac{R_2^2 + R_1^2}{R_2^2 - R_1^2} \right] \pi \rho R_1^2 h$$

where,

M_H = Hydrodynamic mass that depends on the fluid flow when the two bodies move relative to each other,
R_2 = Equivalent radius of storage cell, converting cell width into radius,
R_1 = Equivalent radius of fuel assembly, converting distance between fuel rods of outermost into radius,
h = Length of fuel assembly, and
ρ = Density of fluid.

The calculated hydrodynamic mass according to the above formula is the mass between one cell and fuel assembly. Therefore, the hydrodynamic mass is multiplied by the number of fuel assemblies being stored. Hydrodynamic mass is assigned to the upper and the lower nodes by 1/4 and to the center node by 1/2, respectively.

(2) Rack-to-Rack and Rack-to-Pool Wall

Hydrodynamic masses between rack-to-rack and rack-to-pool wall are calculated based on height of rack, density of fluid and gap of adjacent racks, assuming that the fluid is filled between two objects.

3.1.2.4 Stiffness of Model

Two types of stiffness are used to rack model. First, 3-D elastic beam element is used to represent behavior of racks and fuel assemblies. Secondly, linear friction spring element is used to consider gaps. This spring element is used to calculate the loads in horizontal direction by friction between the pedestal of storage rack and bottom of the pool and impact loads of cell-to-fuel assembly and rack-to-rack, and rack-to-pool wall. Impact phenomena can be represented with a contact element (CONTAC52) of ANSYS (Reference 6). This element is capable of supporting only the compression in the direction normal to the surfaces and the shear (coulomb friction) in the tangential direction. The element has three degrees of freedom for a displacement at each node. A specified stiffness acts in the normal and tangential directions when the gap is closed and not sliding. Figure 3-4 shows the gap elements surrounding one of the typical fuel assemblies and rack masses. The three masses for fuel assemblies and rack are connected in the vertical direction to each other by an axially rigid member.

(1) Impact of Rack Cell-to-Fuel Assembly

A node of fuel assembly beam model and the corresponding node of the rack is connected using CONTAC52 element in order to consider an impact load of the fuel assembly to the rack. The stiffness of this element is applied assuming a series spring connections of the stiffness of fuel assembly's spacer grid and the local stiffness of cell in horizontal direction. However, the stiffness of the fuel assembly only is applied in consideration of conservatism. Fuel assembly/rack cell spring element in Figure 3-4 has a local stiffness (Ki) to account for impact phenomenon of rack cell-to-fuel assembly. The grid stiffness of a fuel assembly is multiplied by the number of fuel assemblies stored.

(2) Support Leg of Rack

Four nodes corresponding to pedestal of rack are connected to pool bottom using CONTAC52 element of ANSYS program. The stiffness for a vertical impact load is applied assuming a series spring connections of the vertical stiffness of rack, embedment plate of pool, and pool concrete. The support pedestal and bottom of pool generate a horizontal direction load by a friction. As a compression load is generated between the pedestal and the pool bottom, the maximum friction load with friction coefficient is considered

with horizontal direction stiffness (Kf) as shown in Figure 3-4. In transient analysis, compression load is calculated at each time step in the analysis.

(3) Impact of Rack-to-Rack and Rack-to-pool wall

The impact of rack-to-rack and rack-to-pool wall is considered as a series spring connections of horizontal stiffness of rack.

3.1.3 Simulation and Solution Methodology

The WPMR analysis is performed to evaluate the displacement and the reaction loads of each rack in the pool, and to establish the presence or absence of specific rack-to-rack or rack-to-wall impacts during a seismic event. The analysis of the fuel storage rack is performed in the procedure of modeling and analysis as follows:

(1) Prepare a 3-D analysis model of all rack modules in the pool for a time-history analysis using ANSYS program (Reference 6). This model includes hydrodynamic effects and nonlinear elements of rack-to-rack and rack-to-fuel to performing an accurate nonlinear simulation and is combined with a fuel pool.

(2) Perform a WPMR dynamic analysis for various conditions of a friction coefficient. Displacements and loads of the storage rack are calculated by ANSYS post-processing.

(3) Perform a kinematic and a stress analysis of racks using the obtained loads and displacements from the dynamic analysis. Calculated stresses are evaluated based on the acceptance criteria in the American Society of Mechanical Engineers (ASME) Code Section III, Subsection NF (Reference 8). In addition, some local evaluations are performed for the bounding case to show that the structural integrity of the fuel assembly remains under all impact loads.

3.2 Acceptance Criteria

The composite dynamic simulation wherein all racks in the pool are modeled is used to determine the loads and displacements for each fuel storage rack in the pool and the relative motion between racks, and to evaluate the potential damage and consequences of inter-rack and rack-wall impact phenomena in the racks.

The NFSRs and the SFSRs are designed as seismic Category I. The structural analysis of fuel storage rack shall be performed for all load conditions on the fuel storage rack into account in accordance with NRC SRP 3.8.4 (Reference 1) and NRC SRP 3.8.5 (Reference 9). This includes loads on fuel storage rack when fuel assembly is normally stored in fuel storage rack; when safe shutdown earthquake occurs; and when the fuel assembly or others handled over the storage rack falls down to the rack. The principal design criteria of the storage rack are shown on subsection 3.2.1 and 3.2.2.

3.2.1 Kinematic Criteria

Because the spent fuel storage rack is not fixed, overturning or sliding of racks can happen due to external load. According to the NRC SRP 3.8.5 (Reference 9), the minimum factor of safety against overturning under the seismic event is 1.5. The rack does not slide off the embedment plates and exhibit a rotation sufficient to bring the center of mass over the corner pedestal.

3.2.2 Stress Limit Criteria

Stress limits must not be exceeded under the required load combinations. The applicable loads and load combinations of structural analysis for the rack are defined in the Table 3-1 based on NRC SRP 3.8.4, Appendix D (Reference 1). The acceptance limits are defined in ASME Code Section III, Subsection NF

(Reference 8), as applicable for Class 3 components support. The APR1400 SFSRs are free-standing; thus, there is no or minimal restraint against free thermal expansion at the base of the rack. Moreover thermal stresses are secondary stress, and have no stipulated stress limits in Class 3 structures or components when acting in concert with seismic loadings. Therefore, thermal loads applied to the racks are not included in the stress combinations involving seismic loadings. ASME Code Section III, Division 1, Subsection NF and Appendix F are applied as stress limits criteria of fuel storage rack for service conditions.

Material properties for analysis and stress evaluation are provided in subsection 3.4.4.

3.2.2.1 Normal Conditions (Level A)

(1) Stress in Tension

The allowable stress in tension on a net section (F_t) is given in NF-3321.1(a)(1).

$$F_t = 0.6\ S_y$$

where,

S_y = yield strength of material at a given temperature.

(2) Stress in Shear

The allowable stress in shear on a net section (F_v) is given in NF-3322.1(b)(1).

$$F_v = 0.4\ S_y$$

(3) Stress in Compression

The allowable stress in compression on a net section (F_a) of austenitic stainless steel is given in NF-3322.1(c)(2).

$$F_a = S_y\ (0.47 - kl/444r)$$

where,

kl/r is less than or equal to 120 for all sections,

l = unsupported length of component,

k = length coefficient which gives influence of boundary conditions, e.g.,

- k = 1 ; simple support both ends,
- k = 2 ; cantilever beam, conservatively use on evaluations,
- k = 0.5 ; clamped at both ends, and

r = radius of gyration of component.

(4) Stress in Bending

The allowable bending stress (F_b) resulting from tension and compression on extreme fibers of box-type flexural members is given in NF-3322.1(d)(4).

$$F_b = 0.60\ S_y$$

(5) Combined Stress (Combined Bending and Compression Loads)

Combined bending and compression load on a net section per NF-3322.1(e)(1) satisfies the following equation.

$$f_a/F_a + C_{mx}f_{bx}/D_xF_{bx} + C_{my}f_{by}/D_yF_{by} < 1.0$$

where,

f_a = Direct compressive stress in the section,
f_{bx} = Maximum bending stress along x-axis,
f_{by} = Maximum bending stress along y-axis,
C_{mx} = 0.85,
C_{my} = 0.85,
D_x = $1 - (f_a/F'_{ex})$,
D_y = $1 - (f_a/F'_{ey})$,
$F'_{ex}, F'_{ey} = (\pi^2 E)/(2.15 (kl/r)_{x,y}^2)$,
and subscripts x and y reflect the particular bending plane.

(6) Combined Stress (Combined Flexure and Tension Loads)

Combined flexure and tension/compression load on a net section satisfies the following equation given in NF-3322.1(e).

$$(f_a/0.6\ S_y) + (f_{bx}/F_{bx}) + (f_{by}/F_{by}) < 1.0$$

(7) Welds

The allowable maximum shear stress on the net section of a weld (F_w) is given in Table NF-3324.5(a)-1.

$$F_w = 0.3\ S_u$$

Where, S_u is the material ultimate strength at temperature. For the area in contact with the base metal, the shear stress on the gross section is limited to $0.4\ S_y$.

3.2.2.2 Upset Conditions (Level B)

The stress limits for Level B are those for Level A multiplied by the stress limit factor specified in Table NF-3312.1(b)-1 (Reference 8). The stress limit factors for Level B are larger than those for Level A. However, allowable stress of Level A is used for Level B for conservatism.

3.2.2.3 Faulted (Abnormal) Conditions (Level D)

Article F-1334 of ASME Code Section III, Appendix F (Reference 8) states that the limits for the Level D condition are the smaller of 2 or $1.167\ S_u/S_y$ times the corresponding limits for the Level A condition if $S_u > 1.2\ S_y$, or 1.4 if S_u is less than or equal to $1.2\ S_y$ except for requirements specifically listed below. S_u and S_y are the ultimate strength and the yield strength at the specified rack design temperature.

Exceptions to the above general multiplier are the following:

(1) The tensile stress on the net section shall not exceed the lesser of $1.2\ S_y$ and $0.7\ S_u$.

(2) The shear stress on the gross section shall not exceed the lesser of $0.72\ S_y$ or $0.42\ S_u$. In the case of the austenitic stainless steel material used here, $0.72\ S_y$ governs.

(3) Combined axial compression and bending - The equations for Level A conditions shall apply except that F_a = 2/3 x Buckling Load, and F'_{ex} and F'_{ey} may be increased by the factor 1.65.

(4) For welds, the Level D allowable weld stress is not specified in Appendix F of the ASME Code. Therefore, a limit for weld throat stress is used conservatively as follows:

$$F_w = (0.3\ S_u) \times \text{Factor}$$

where, Factor = (Level D shear stress limit)/(Level A shear stress limit)

$= 0.72 \times S_y / 0.4 \times S_y = 1.8$

For 304L stainless steel, 1.2 times the yield strength is less than the ultimate strength and the value of 1.167 S_u/S_y is equal to 3.6 so that 2.0 is used for the multiplier.

3.2.3 Dimensionless Stress Factors

Dimensionless stress factors are calculated by the ratio of the calculated stress to the allowable stress for the combined and the individual loads according to ASME Code Section III, Division 1, Subsection NF. In case the calculated stress factor is less than 1.0, it is considered to meet stress limit requirements for each service condition. In this report, a stress factor as described below is calculated using load combination for each service condition.

FACT 1 = Stress factor of member subject to combined bending and compression (as defined in subsection 3.2.2.1(5)).
FACT2 = Stress factor of member subject to combined flexure and tension (or compression) (as defined in subsection 3.2.2.1(6)).
FACT3 = Stress factor of gross shear on a net section.

3.3 Assumptions

The following assumptions are used in the WPMR dynamic analysis:

(1) Fluid damping is conservatively neglected, since it yields larger rack displacement.

(2) Sloshing effect of spent fuel pool surface is neglected because the rack is deeply submerged in the fluid.

(3) Fuel assembly is considered as 3-D elastic beam with concentrated masses at the upper and lower ends and the middle point of the rack. Each concentrated mass has a degree of freedom in horizontal direction. Vertical movement of fuel assembly is assumed to be tied up to vertical movement of the rack baseplate.

(4) When earthquake occurs, the rack is affected by irregular movement of every single fuel assembly. For conservative evaluation, all the fuel assemblies within the rack rattle in unison throughout the seismic event, which obviously exaggerates the contribution of impact against the cell wall.

3.4 Input Data

3.4.1 Rack Data

Dimensions and weight of the new and the spent fuel storage racks used in the analysis are in accordance with the design drawings (References 10 and 11) and are summarized in the Tables 2-1, 2-2 and 3-2.

3.4.2 Fuel Assembly Data

Dimensions and weight of the fuel assembly used in the analysis are based on the pressurized water reactor (PWR) PLUS7 fuel assembly data (Reference 12) and are summarized in the Table 3-3.

3.4.3 Structural Damping

Rayleigh damping is used to specify mass (M) and stiffness (K) proportional damping (C):

$$C = \alpha \times M + \beta \times K$$

The constants α and β are calculated in the range of the lowest and highest frequencies of interest in the dynamic analysis (Reference 7). M corresponds to real mass of the real-fuel system and does not include any hydrodynamic mass. Only material damping for the fuel and rack is used in calculating the damping matrix C. The design basis damping value for the NFSRs and the SFSRs is conservatively used as 3% for SSE event in accordance with the regulatory guide (RG) 1.61 (Reference 13) for welded steel.

3.4.4 Material Data

Material properties of fuel assembly are taken from the PWR PLUS7 fuel assembly data (Reference 12) as shown in the Table 3-3. In addition, those of rack are obtained from ASME Code Section II, Part D (Reference 14) as shown in the Table 3-4. The values listed correspond to a design temperature of 93.3 ^{o}C (200 ^{o}F).

3.5 Computer Codes

The computer codes listed in Table 3-5 are used in the dynamic analysis.

3.6 Dynamic Simulations

Four simulations shown in Table 3-6 are performed for the new and the spent fuel pool racks to investigate the structural integrity of each rack. SSE event is considered as loading conditions for the racks. The storage rack configurations at the full loading are considered in the dynamic simulations. To consider the effort of the friction coefficient between pedestal and embedment plate as discussed in subsection 3.1.2, simulations are performed by varying the friction coefficient with upper and lower bound values, and a mean value. The nonlinear dynamic analyses for dynamic simulations of the NFSRs and the SFSRs are performed using the ANSYS (Reference 6) finite element program.

3.7 Results of Analyses

3.7.1 Time History Simulation Results

The loads and the displacements by dynamic simulations are summarized in Table 3-7 through Table 3-10.

3.7.1.1 Displacements of Rack

The maximum relative displacement of the adjacent racks which means to be closer to each other is 42.8 mm (1.684 in) in north-south (N-S) direction between A1-2 and A2-2 racks at 10.12 seconds and 4.8 mm (0.187 in) in east-west (E-W) direction between B9 and B10 racks at 17.13 seconds. The minimum gap for the cell-to-cell of Region I is 60.0 mm (2.36 in), and that of Region II is 30.0 mm (1.18 in). Therefore, there is no impact on the rack cells by each other, because the maximum relative displacements of racks are smaller than the installation gap. The maximum displacement for upper end of spent fuel storage rack is 94.9 mm (3.735 in) in E-W direction for B6-2 rack at 14.424 seconds as shown in Table 3-7. The minimum gap of the outmost rack and the pool wall is 716.6 mm (28.21 in) in N-S direction and 835.4 mm (32.89 in) in E-W direction as shown in Figure 2-4. Therefore, there is no impact on the outmost rack by the pool wall, because the maximum displacement of the rack is smaller than the installation gap. Actually, impact on rack-to-rack occurs at baseplate of the SFSRs because the installed racks are in contact with each other. The maximum impact loads generated at the NFSRs and the SFSRs are summarized in Table 3-10.

The maximum rotations of the rack are obtained from a post-processing of the rack time history response output. The SFR and the NFR should not exhibit rotations sufficient to cause the rack to overturn (i.e., ensure that the rack does not exhibit a rotation sufficient to bring the center of mass over the corner

pedestal). The greatest horizontal displacement in the rack is calculated as 94.9 mm (3.735 in) for the rack module B6-2 as shown in Table 3-7. Based on the width and height of rack B6-2, the rotation required to produce incipient tipping for this rack is approximately equal to $\tan^{-1}[(1,805/2) / (4,775/2)] = 20.6^{o}$. Whereas, the actual rotation due to the largest displacement may be computed as $\tan^{-1}[(94.9) / (4,775)] = 1.2^{o}$. The safety factor against overturning is about $20.6^{o} / 1.2^{o} = 17$, which is greater than the acceptance criteria of 1.5. Therefore, the overturning of rack module does not occur.

3.7.1.2 Support Pedestal Loads of Rack

The maximum horizontal and vertical loads generated on support pedestal with the application of SSE loads are summarized in Table 3-8 and Table 3-9, and used to structural integrity evaluation of support pedestal and rack. The maximum horizontal and vertical loads for NFSR pedestal are calculated as 756.2 kN (170,000 lbf) and 249.0 kN (55,980 lbf) and those for SFSR pedestal are calculated as 529.3 kN (119,000 lbf) and 662.8 kN (149,000 lbf), respectively.

3.7.1.3 Impact Loads

The impact loads for fuel-to-cell wall, rack-to-rack and rack-to-wall on the NFP and SFP are calculated as follows:

(1) Fuel-to-Cell Wall

The maximum impact loads of fuel-to-cell wall on the NFSRs and the SFSRs are 39.0 kN (8,777 lbf) and 111.2 kN (25,000 lbf), respectively, which are as shown in Table 3-10. In addition, the maximum impact loads on fuel support grid of the NFSRs and the SFSRs are 3.5 kN (798 lbf) and 10.1 kN (2,273 lbf), respectively.

(2) Impacts of Rack-to-Rack and Rack-to-Pool Wall

Generally, the racks are installed together as closely as possible. The prominent baseplate of the fuel storage rack for the APR1400 design is installed almost in contact with the adjacent baseplate. According to the analysis result, the impact occurs not between the pool wall and the upper part of the rack, but between the baseplate of racks. The maximum impact load at the baseplate of rack is calculated as 1,343.4 kN (302,000 lbf) as shown in Table 3-10.

3.7.2 Fuel Structural Evaluation

The impact loads on the fuel assembly should not lead to damage of the fuel. Damage of the fuel are evaluated for structural elements of a fuel assembly including the fuel rod cladding which are stressed beyond the material allowable limits such that the fuel rods are no longer able to provide confinement for contained radioactive fission materials. In addition, an evaluation considering pertinent failure mode such as bucking should be performed to demonstrate that the structural elements of the fuel assembly will not exceed the material allowable limits. Therefore, the lateral impact load on the spent fuel assembly is evaluated for two acceptance criteria; fuel spacer grid buckling and fuel cladding yield stress.

The maximum impact load applying on fuel assembly is evaluated for 111.2 kN (25,000 lbf) as shown in Table 3-10. Therefore, the maximum acceleration load that the rack imparts on the fuel assembly can be conservatively calculated as follows:

$$a = \frac{F}{w} = 17.3 \text{ g}$$

where,

a = Maximum lateral acceleration in g's,
F = Maximum fuel-to-cell wall impact load per cell (= 111.2 kN (25,000 lbf)), and

w = Weight of one fuel assembly (= 657 kgf (1,448 lbf)).

The structural integrity of fuel assembly is evaluated for the maximum lateral acceleration load (17.3 g).

3.7.2.1 Buckling Evaluation of Fuel Spacer Grid

The lateral impact loads on a single fuel grid spacer is compared against its buckling capacity, which is derived from the data in SANDIA Report SAND90-2406 (Reference 15). This report provides an analysis which predicts the onset of buckling of the pressurized water reactor (PWR) spacer grid at 66.8 N (15 lbf) of load per fuel rod. The initial loading from the fuel rods on a lateral impact compresses the leaf springs onto the spacer grid frame. And then the spacer compresses the springs to the bottom, resulting in a deflection of the spacer grid frame. The spacer grid frames provide resistance to the point where the frame begins to buckle. After buckling, the frame offers a minimal resistance to further load. The objective of this analysis is to demonstrate that the spacer grids do not buckle and consequently rod-to-rod contact does not occur.

The fuel assembly spacer grid model for the PWR 15 x 15 fuel assemblies is based on the nonlinear spring element of the fuel assembly spacer grid obtained from the analysis of a single spacer grid cell. The basis of this cell model is verified through extensive modeling of entire spacer grid frames, as described in the SANDIA report (Reference 15). Appendix III.5.3 of the SANDIA report (Reference 15) shows the deflected shape from the PWR 15 x 15 single-bay slice model analysis and the force deflection spring elements developed for the Babcock and Wilcox (B&W) assembly models used to simulate the spacer grid for the two-dimensional side drop assembly analyses. Each spring element of PWR 15 x 15 fuel assemblies will accrue the force from the all rods adjacent to the spring of interest, and so the buckling force of 934 N (210 lbf) for an individual cell is equivalent to a force of 66.8 N (15.0 lbf) in each rod that buckles at the last cell in the row. The buckling capacity of the spacer grid is inversely proportional to the square of the cell size, i.e., the length of the unsupported column, and the cell size is directly related to the fuel rod pitch.

Since the cells in the PWR 16 x 16 spacer grids for the APR1400 design are smaller than the PWR 15 x 15 spacer grids, the smaller cells are more resistant to buckling. The ratio of rod pitch for each fuel assembly is calculated as follows:

$$\text{Ratio} = \frac{P15\times15}{P16\times16} = \frac{1.443}{1.285} = 1.123$$

Therefore, the critical buckling load of the fuel spacer grid for the APR1400 design is 934 x $(1.123)^2$ = 1,178 N (265 lbf). Furthermore, the mass of the fuel assembly channel does not contribute to the buckling loads on the spacer grid, so only the fuel rod mass is considered in this analysis. The fuel rod mass is applied as 0.61 kg/m (0.034 lbm/in) from Table 3-3. The load imposed on a cell in the spacer grid is 1/2 the mass of the fuel rod on each side of the spacer cell or 2 x (359.4 / (2 x1,000)) (0.61) (17.3 g) = 37.2 N (8.4 lbf), and the combined load from 15 fuel rods adjacent to the critical cell is 15 x 37.2 = 558 N (125 lbf).

3.7.2.2 Stress Evaluation of Fuel Cladding

The maximum lateral acceleration acting on the fuel mass is used to calculate a load uniformly distributed over a single fuel rod modeled as a beam simply supported by the spacer grids, and the maximum fuel rod length between the spacer grids is 359.4 mm (14.148 in) as shown in Table 3-3.

The uniformly distributed load on the fuel rod is calculated as follows:

$q = a \times W_{fuel} = 17.3 \times 0.61 = 103.4$ N/m (0.59 lbm/in)

where,

a = Maximum lateral acceleration in g's (=17.3 g), and

W_{fuel} = Fuel assembly rod mass per unit length (= 0.61 kg/m).

The maximum bending moment for uniform load is calculated as

$M = (q \times L_{spacer}^2) / 8 = (103.4)(359.4/1{,}000)^2 / 8 = 1.67$ N-m (14.77 lbf-in)

where,

L_{spacer} = Maximum fuel rod length between spacer grids (=359.4 mm (14.148 in)).

The resulting maximum bending stress in the fuel cladding is calculated as 49.4 MPa (7,166 psi) from equation below.

$$\sigma_b = \frac{M \cdot R_o}{I} = 49.4 \text{ MPa (7,166 psi)}$$

where,

R_o = Outer radius of fuel rod (= 4.75 mm (0.187 in)), and
I = Moment of inertia of fuel rod cladding (= 160.4 mm^4 (3.853 x 10^{-4} in^4))

As results for fuel assembly evaluation, both the maximum impact load on an individual fuel grid spacer cell and the bending stress induced in the fuel rod cladding due to the maximum lateral acceleration are summarized in Table 3-11. The structural integrity of the stored fuel assemblies under the SSE event is assured, because the safety factors are greater than 1.0.

3.7.3 Rack Structural Evaluation

To insure that the fuel racks have adequate safety margins, all stress evaluations for the fuel racks are performed based on the worst-case results from four simulations. In this section, the structural integrity of weld and each part of rack is evaluated by using the maximum loads in vertical and horizontal direction calculated by time-history analysis of fuel storage rack.

3.7.3.1 Stress Factors of Rack

With time-history analysis results available for pedestal normal and lateral interface forces, the limiting bending moment and shear force at the baseplate-to-pedestal interface may be computed as a function of time. In particular, maximum values for the stress factors which are defined on section 3.2 can be determined for every pedestal in the rack. Using this information, the structural integrity of the pedestal can be assessed.

The net section maximum bending moments and shear forces can also be determined at the bottom of the cellular structure. From these loads, the stress factors for the NFSRs and the SFSRs cellular cross section just above the baseplate can be also determined in the rack. These locations are the most heavily loaded net sections in the structure so that satisfaction of the stress factor criteria at these locations ensures that the overall structural criteria set forth in section 3.2 are met.

The maximum pedestal stress factors for the NFSRs and the SFSRs are 0.538 and 0.436, respectively and are less than the allowable of 1.0. The maximum cell wall stress factors for the NFSRs and the SFSRs are 0.054 and 0.314, respectively, and are less than the allowable of 1.0. Therefore, the rack cells and the support pedestals are able to maintain their structural integrity under the worst loading conditions.

The maximum stress factors for the rack cells and the support pedestals are less than the allowable of 1.0 for the governing faulted condition examined as shown on Table 3-12.

3.7.3.2 Pedestal Thread Stress Evaluation

The integrity for the support pedestal thread is evaluated for the maximum load of support pedestal in vertical direction as shown in Table 3-9. Using this load, the maximum shear stress of thread in the engagement region is calculated. The allowable shear stress of SA-240 Type 304L material for Level D condition is the lesser of 0.72 S_y = 106.2 MPa (15,408 psi) or 0.42 S_u = 191.4 MPa (27,762 psi) as stated on subsection 3.2.2. Therefore, the former criteria controls, and the calculated shear stress of pedestal thread is as shown on Table 3-13.

3.7.3.3 Stresses on Welds

Weld locations of the NFSRs subjected to SSE loading are at the bottom of the rack at the cell-to-baseplate connection, and at the top of the pedestal support at the baseplate connection. In addition, weld locations for the SFSRs are at the bottom of the rack at the cell-to-baseplate connection, at the top of the pedestal support at the baseplate connection, and at cell-to-cell connections. The maximum values of resultant loads are used to evaluate the structural integrity of these welds. The calculated stresses on welds of rack are summarized in Table 3-13.

(1) Cell-to-Baseplate Weld

As given in ASME Code Section III, Subsection NF, for Level A or B conditions, an allowable shear stress of a weld is 0.3 S_u = 136.7 MPa (19,830 psi) conservatively based on the base metal material. As stated in subsection 3.2.2, the allowable weld stress may be increased for Level D by the ratio of 1.8, giving an allowable of 0.54 S_u = 246.1 MPa (35,694 psi).

Weld stresses on the cell-to-baseplate are determined through the use of a simple conversion factor (ratio) applied to the corresponding stress factor in the adjacent rack material. This stress factor is discussed in section 3.2, and given in the Table 3-12. The conversion factor (ratio) values are developed from consideration of the differences in material thickness and length versus weld throat dimension and length, as follows:

$$\text{Ratio} = [(220 + 2.5) \times 2.5)] / (180 \times 2.5 \times 0.707) = 1.75 \text{ (for the SFSRs)}$$

where, Inner cell dimension (220 mm (8.66 in)), Cell wall thickness (2.5 mm (0.098 in)), Weld length (180 mm (7.09 in)), and Weld thickness (= 2.5 x 0.707 = 1.767 mm (0.069 in)) are used.

For the NFSRs, the cell wall thickness and weld thickness are 6.0 mm (0.236 in) and 4.24 mm (0.167 in), respectively. The conversion factor (ratio) for the NFSRs is calculated as 1.54.

The highest predicted cell-to-baseplate weld stress is conservatively calculated based on the highest FACT2 for the rack cell region tension stress factor and FACT3 for the rack cell region shear stress factor. The maximum stress factors used do not all occur at the same time instant and the shear stress factors are the maximum for all load conditions. These cell wall stress factors are converted into actual stress on the weld of cell-to-cell as follows:

$(FACT2 + FACT3) \times (2 \times 0.6 \times S_y) \times Ratio = (0.314 + 0.07) \times (2 \times 0.6 \times 147.55) \times 1.75 = 119.0$ MPa (17,257 psi)

The 2.0 multiplier value is used to adjust the Level A allowable to the Level D allowable, as discussed in subsection 3.2.2. The calculated stress value is less than the allowable weld stress value of 246.1 MPa (35,694 psi). Therefore, all weld stresses between the cell wall and the baseplate are acceptable.

(2) Baseplate-to-Pedestal Weld

The weld stress on the baseplate-to-pedestal is conservatively evaluated using the maximum pedestal load of the NFSR and the dimension of support pedestal welds of spent fuel storage rack. The weld between baseplate and support pedestal is checked using finite element analysis to determine that the maximum stress is 124.1 MPa (17,992 psi) under a Level D condition. This calculated stress value is well below the Level D allowable of 246.1 MPa (35,694 psi). Therefore, all weld stresses between baseplate and support pedestal are acceptable.

(3) Cell-to-Cell Weld

Stress of cell-to-cell weld is calculated by combination the shear stress due to horizontal load acting on rack and the shear stress due to impact load of rack cell-to-fuel assembly. Cell-to-cell connections are by a series of connecting welds along the cell height. Stresses in storage cell to cell welds develop due to fuel assembly impacts with the cell wall. These weld stresses are conservatively considered by assuming that fuel assemblies in adjacent cells are moving out of phase with one another so that impact loads in two adjacent cells are in opposite directions and are applied simultaneously. This load application tends to separate the two cells from each other at the weld. Stress of cell-to-cell weld is combined by the square root of the sum of the squares (SRSS) method for the shear stress due to horizontal load acting on rack and the shear stress due to impact load of rack cell-to-fuel assembly. The calculated stresses of the cell-to-cell weld and the base metal shear are well below the allowable, and the results are summarized in Table 3-13.

3.7.3.4 Local Stress Evaluation

(1) Cell Wall Impact

The maximum impact loads of fuel-to-cell wall on the NFSRs and the SFSRs are 3.5 kN (798 lbf) and 10.1 kN (2,273 lbf), respectively, which are as shown in Table 3-10. The evaluation for cell wall for impact is performed to guarantee that local impact does not affect criticality of stored fuel. Integrity of local cell wall is evaluated conservatively using the peak impact load. Limit impact load to induce overall permanent deformation is calculated by plastic analysis. The cell walls of the new and the spent fuel storage racks endure the side load of the maximum 273.2 kN (61,410 lbf) and 47.4 kN (10,660 lbf), respectively (Reference 7). Therefore, the cell wall of racks satisfies the requirement with the maximum impact loads less than the allowable loads.

(2) Cell Wall Buckling

The allowable local buckling stresses of cell walls for fuel storage rack are obtained by using classical plate buckling analysis on the lower portion of the cell walls. A critical bucking stress of cell walls can be calculated by following equation.

$$\sigma_{cr} = \frac{\beta \pi^2 E t^2}{12 b^2 (1 - \nu^2)}$$

Where, E (Young's modulus) = 1.896E+05 N/mm^2(27.5E+06 psi), υ (Poisson's ratio) = 0.3, t (Cell Thickness) = 2.5 mm(0.098 in), b (Cell width) = 220 mm(8.66 in), and β (Value of coefficient) = 4.0 which is indicated for a long plate (Reference 16).

For the given data above, the critical buckling stress (σ_{cr}) is conservatively calculated as 87.8 MPa (12,731 psi) for all racks. It should be noted that this calculation is based on the applied stress being uniform along the entire length of the cell wall. In the actual fuel rack, the compressive stress comes from consideration of overall bending of the rack structures during a seismic event and as such is negligible at the rack top. In the simulation, the maximum compressive stress due to overall bending is generated near baseplate. This local buckling stress limit is not violated anywhere in the body of the rack modules, since

the maximum compressive stress in the outermost cell is σ = 2 x 0.6 x 147.5 x FACT2 (from Table 3-12 with FACT2 = 0.314) = 55.6 MPa (8,061 psi) and is within the allowable value of 87.8 MPa (12,731 psi). Therefore, a buckling of the rack cell wall does not occur.

(3) Secondary Stress by Temperature Effects

The temperature gradients across the rack structure caused by differential heating effects between one or more filled cells and one or more adjacent empty cells are considered. The worst thermal stress in a fuel rack is obtained when a storage cell has a fuel assembly generating heat at the maximum postulated rate and the surrounding storage cells contain no fuel. The thermal stress is classified as secondary stress on the ASME Code Section III, Division 1. Therefore, it is independently evaluated without combining with primary stress of other load condition.

A conservative estimate of the weld stresses along the length of an isolated hot cell is obtained by considering a beam strip uniformly heated by ΔT = 36 ^{o}C (65 ^{o}F), and restrained from growth along one long edge. The temperature rise envelops the difference between the maximum local spent fuel pool water temperature (68.3 ^{o}C (=155 ^{o}F) bounding) inside a storage cell and the bulk pool temperature (49.4 ^{o}C (= 121 ^{o}F)) based on the thermal-hydraulic analysis of the spent fuel pool. The maximum shear stress due to temperature change for isolated hot cell weld is calculated as follows:

$$\tau_{max} = E \times \alpha \times \Delta T$$

where, E = 1.896E+05 N/mm^2(27.5E+06 psi), α = 9.5E-06 in/in-^{o}F, and ΔT = 36 ^{o}C(65 ^{o}F).

The maximum shear stress due to the temperature gradient for an isolated hot cell is calculated as 117.1 MPa (16,981 psi). Since this thermal stress is classified as secondary stress, the allowable shear stress criteria for Level D condition (0.42 S_u = 191.4 MPa (27,762 psi)) is used as the limits of allowable. Therefore, the maximum shear stress due to the temperature gradient is acceptable.

Table 3-1 Load Combinations for Rack Analysis

Load Combination	Acceptance Limit
D + L D + L + T_o D + L + T_o + E	ASME Code Section III, Subsection NF Level A service limits for Class 3
D + L + T_a + E D + L + T_o + P_f	ASME Code Section III, Subsection NF Level B service limits for Class 3
D + L + T_a + E'	ASME Code Section III, Subsection NF Level D service limits for Class 3
D + L + F_d	The functional capability of the fuel racks should be demonstrated.

Where,

D : Dead weight including fuel assembly weight.

L : Live load (not applicable for the fuel rack, since there are no moving objects in the rack load path). Note that it is accepted practice to consider the fuel weight as a dead weight.

E : Operating Basis Earthquake (OBE).

E' : Safe Shutdown Earthquake (SSE).

T_o= Differential temperature induced loads, based on the most critical transient or steady state condition under normal operation or shutdown conditions.

T_a= Highest temperature associated with the postulated abnormal design conditions.

F_d= Force caused by the accidental drop of the heaviest load from maximum possible height.

P_f= Upward force on the racks caused by a postulated stuck fuel assembly. This force may be caused at any angle between horizontal and vertical.

Table 3-2 Rack Size and Weight

Rack Modules(*)		Array Size	Weight, kgf (lbf)
NFSR		7 x 8	
SFSR	A1-1, A1-2, A1-3 & A1-4	8 x 8	
	A2-1 & A2-2	6 x 8	
	B1 B2-1, B2-2, B2-3 B3, B4 B5-1, B5-2, B5-3, B5-4, B5-5, B5-6 B6-1, B6-2, B6-3 B7, B8 B9, B10	8 x 8	
	C1, C2, C3 & C4	8 x 7	

TS

(*) Refer to Figure 2-1 and Figure 2-4

Table 3-3 Data of Fuel Assembly

Parameter	Data (*)
Weight of Fuel Assembly, kg (lb)	
Grid width of Fuel Assembly, mm (in)	
Max. Fuel Rod Length between Spacer Grid, mm (in)	
Mass of Fuel Rod, kg/m (lbm/in)	
Outer Diameter of Fuel Rod, mm (in)	
Inner Diameter of Fuel Rod, mm (in)	
Clad Thickness, mm (in)	
Area Moment of Inertia of Fuel Rod Clad, mm^4 (in^4)	
Young's Modulus of Fuel Rod Clad, MPa (psi) at 93.3 ^oC (200 ^oF)	
Yield Strength of Fuel Rod Clad, MPa (psi) at 93.3 ^oC (200 ^oF)	
Total Grid Number, ea	

TS

(*) All of the dimensions are nominal values.

Table 3-4 Material Properties

Part	Material	Young's Modulus (E) MPa (psi)	Yield Strength (S_y) MPa (psi)	Ultimate Strength (S_u) MPa (psi)
Rack	SA-240 Type 304L	189,605 (27.5E+06)	147.5 (21,400)	455.7 (66,100)
Support Pedestal (Upper Part)	SA-240 Type 304L	189,605 (27.5E+06)	147.5 (21,400)	455.7 (66,100)
Pedestal Bolt Part	SA-564 Grade 630 (Hardened at 1100 ^oF)	191,674 (27.8E+06)	732.9 (106,300)	965.3 (140,000)

Table 3-5 Computer Codes used in Mechanical Analysis

No.	Code	Version	Remark
1	ANSYS	10.0	ANSYS is an industry-standard general purpose Finite Element Analysis (FEA) program. The elements and options used in this analysis are well-established and fully verified.
2	ATIGEN	0	Generate artificial time histories from input response spectra data and based on NRC Standard Review Plan 3.7.1 which requires comparison of PSD (Power Spectral Density) of original (target) with regenerated results.
3	STCOR	0	Check the statistical independence of the generated artificial time histories from given response spectra

Table 3-6 List of Simulation

No.	Rack	Fuel Storage	Seismic Load	COF
1	NFSR	Full	SSE	N/A
2	SFSR	Full	SSE	0.2
3		Full	SSE	0.5
4		Full	SSE	0.8

Table 3-7 Displacement of Racks

1) Maximum Displacement (Horizontal direction)

Rack	Displacement, mm (in)	Time (sec)	Direction	Rack Number	COF
NFSR	10.8 (0.425)	3.405	N-S	N/A	N/A
SFSR	94.9 (3.735)	14.424	E-W	B6-2	0.2
	47.2 (1.858)	14.305	E-W	B10	0.5
	28.8 (1.134)	14.185	E-W	B5-6	0.8

2) Maximum Relative Displacement (Direction to be close to each rack)

Rack		Relative Displacement, mm (in)	Time (sec)	Direction	Rack Number	COF
SFSR	Region I Racks	42.8 (1.684)	10.12	N-S	A1-2 to A2-2	0.2
		20.4 (0.804)	17.98	N-S	A1-2 to A2-2	0.5
		13.6 (0.536)	10.09	N-S	A1-2 to A2-2	0.8
	Region II Racks	4.8 (0.187)	17.13	E-W	B9 to B10	0.2
		3.4 (0.133)	5.105	E-W	B1-1 to B2-1	0.5
		4.6 (0.179)	4.261	E-W	C3 to C4	0.8

Table 3-8 Maximum Loads on Rack Module

Rack	Type (Cell Array)		Horizontal direction, kN (lbf)	Vertical direction, kN (lbf)	COF
NFSR	7 x 8		2,282.4 (513,100)	996.0 (223,900)	N/A
SFSR	A1 type	8 x 8	1,699.2 (382,000)	2,655.6 (597,000)	0.8
	A2 type	6 x 8	1,441.2 (324,000)	2,268.6 (510,000)	0.8
	B type	8 x 8	2,095.1 (471,000)	2,633.3 (592,000)	0.8
	C type	8 x 7	1,690.3 (380,000)	2,366.5 (532,000)	0.8

Table 3-9 Maximum Loads on Single Pedestal

Rack	Type (Cell Array)		Horizontal Direction, kN (lbf)		Vertical direction, kN (lbf)	COF
			E-W	N-S		
NFSR	7 x 8		756.2 (170,000)	660.1 (148,400)	249.0 (55,980)	N/A
SFSR	A1 type	8 x 8	444.8 (100,000)	229.1 (51,500)	662.8 (149,000)	0.8
	A2 type	6 x 8	304.7 (68,500)	326.9 (73,500)	569.4 (128,000)	0.8
	B type	8 x 8	529.3 (119,000)	269.1 (60,500)	658.3 (148,000)	0.8
	C type	8 x 7	423.9 (95,300)	175.3 (39,400)	591.6 (133,000)	0.8

Table 3-10 Impact Loads on Rack

Rack	Location	Direction	Impact Load, kN (lbf)	Rack Number (Module)	Impact Load per Cell (1), kN (lbf)	Impact Load of Fuel Support Grid (2), [kN (lbf)]	COF
NFSR	Cell-to-Fuel Assembly	E-W	2,053.3 (461,600)	-	36.7 (8,243)	3.3 (750)	-
		N-S	2,186.3 (491,500)	-	39.0 (8,777)	3.5 (798)	-
SFSR	Rack-to-Rack Baseplate	-	1,343.4 (302,000)	C1 (8x7)	-	-	0.2
	Cell-to-Fuel Assembly	E-W	7,117.2 (1,600,000)	A1-1 (8x8)	111.2 (25,000)	10.1 (2,273)	0.8
		N-S	5,293.4 (1,190,000)	A1-2 (8x8)	82.7 (18,594)	7.5 (1,690)	0.8

Notes:

(1) Impact load per cell = Side impact load/Number of stored fuel

(2) Impact load of fuel support grid = Impact load per cell/ Number of support grid

Table 3-11 Stress Evaluation for Fuel Assembly

Location	Category	Calculated Value	Allowable Limit	Safety Factor (-)
Fuel grid spacer	Buckling Load	558 N (125 lbf)	1,178 N (265 lbf)	2.1
Fuel rod cladding	Bending Stress	49.4 MPa (7,166 psi)	540.3 MPa (78,365 psi)	10.9

Table 3-12 Maximum Stress Factors of Rack

Rack		Pedestal Stress Factors			Cell Wall Stress Factors			COF
		FACT1	FACT2	FACT3	FACT1	FACT2	FACT3	
NFSRs		0.476	0.538	0.389	0.05	0.054	0.031	0.8
SFSRs	Region I Racks	0.41	0.436	0.219	0.149	0.16	0.032	0.8
	Region II Racks	0.337	0.357	0.236	0.295	0.314	0.07	0.8

Notes:
(1) Dimensionless stress factors, FACT1, FACT2, and FACT3, are stated on subsection 3.2.3.

Table 3-13 Stress Evaluation for Fuel Racks

Region	Type	Calculated Stress, MPa (psi)	Allowable Stress, MPa (psi)	Safety Factor (-)
Rack Cell-to-Baseplate	Weld	203.7 (29,545)	246.1 (35,694)	1.21
Baseplate-to-Pedestal	Weld	124.1 (17,992)	246.1 (35,694)	1.98
Cell-to-Cell	Weld	45.4 (6,581)	246.1 (35,694)	5.42
	Base Metal Shear	32.1 (4,653)	118.0 (17,120)	3.68
Pedestal Thread	Shear	40.4 (6,507)	106.2 (15,408)	2.63

Notes:
(1) Stresses on weld of the baseplate-to-support pedestal of the rack are conservatively evaluated by applying the maximum support loads acting on the NFSRs as shown on Table 3-9 to the weld of the support pedestal of the SFSRs.

TS

Figure 3-1 Dynamic Analysis Model of NFSR

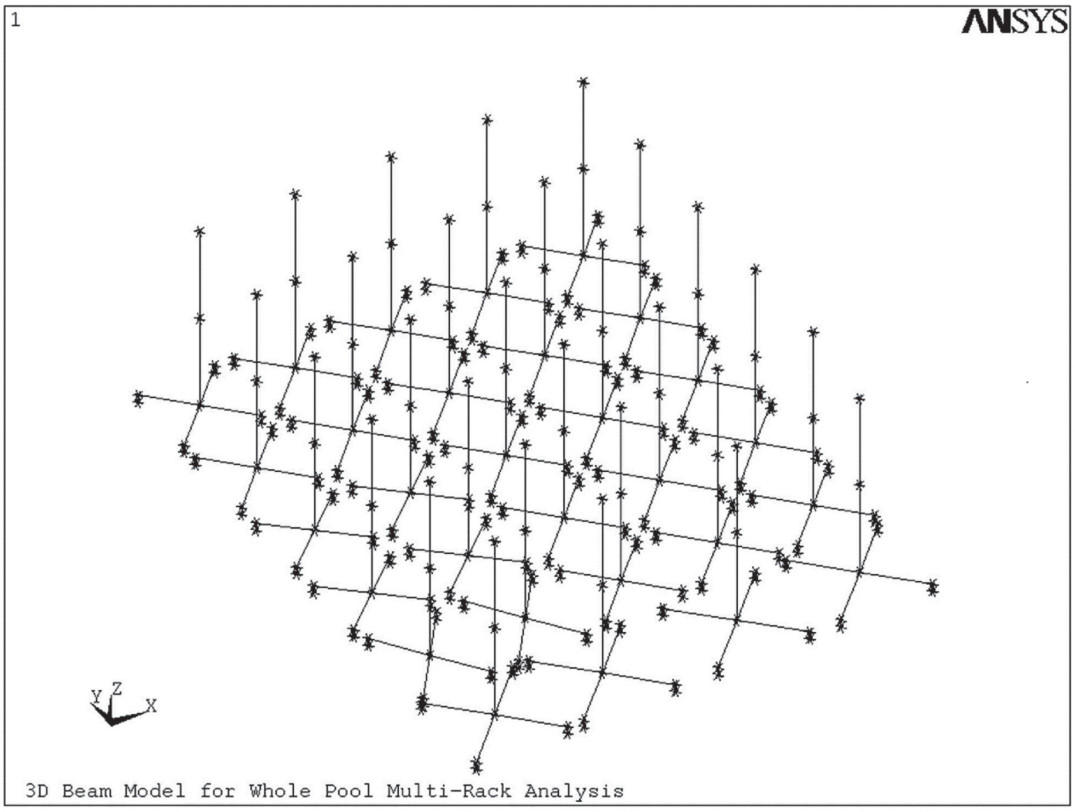

Figure 3-2 Dynamic Analysis Model for Whole Pool Multi-Rack

Figure 3-3 Dynamic Analysis Model of SFSR

TS

Figure 3-4 Schematic of Spring Elements used for SFSR

4 MECHANICAL ACCIDENTS ANALYSIS

This chapter presents the structural integrity evaluation for new and spent fuel storage racks under the mechanical accident conditions. Mechanical accidents are analyzed and their consequences are evaluated for all the new and the spent fuel storage racks. The accident analyses demonstrate that the racks designed for installation at the APR1400 design meet the acceptance criteria which are specified on NRC SRP 3.8.4, appendix D (Reference 1).

4.1 Description of Mechanical Accidents

The NRC SRP 3.8.4, appendix D (Reference 1) specifies that the design of the racks must ensure the functional capability should be demonstrated under the accidental drop of the heaviest load from the possible weight. Four categories of mechanical accidents are considered. The mechanical accidents, which are three types of dropped fuel assembly accident and one stuck fuel assembly accident, are described as follows:

(1) Straight Shallow Drop (Scenario 1)

The fuel assembly along with the handling tool, which total weight is 1,100 kgf (2,425 lbf), hereinafter called the "dropping mass", drops down from a height of 0.61 m (2 ft) above the top of the fuel rack and impacts on a top edge of the rack. Schematic of the straight shallow drop is shown as Figure 4-1.

(2) Straight Deep Drops (Scenarios 2 & 3)

The dropping mass drops down from a fuel bottom height of 0.61 m (2 ft) above the top of the fuel rack. The falling assembly enters a storage cell, and impacts the rack baseplate. The deep drop accident can be classified into two scenarios which are drop in an interior cell away from the support pedestals (Refer to Figure 4-2) and drop through the cell located above a support pedestal (Refer to Figure 4-3).

(3) Stuck Fuel Assembly (Scenario 4)

A “stuck fuel” accident is analyzed to determine the damage of the rack due to a tensile force of 2,268 kgf (5,000 lbf) applied to the rack by a stuck fuel assembly.

4.2 Acceptance Criteria

For mechanical accidents above, the acceptance criteria to ensure the functional capability of the racks are described as shown below:

(1) Straight Shallow Drop (Scenario 1)

For the postulated shallow drop event, the depth of damage to the impacted cell walls must be demonstrated to remain limited to the portion of the cell above the top of the "poison zone", which is the elevation of the top of the neutron absorber. This will ensure that the configuration analyzed in the criticality evaluation remains valid. The distance measured from the top of the rack to the upper boundary of the "poison zone" is 0.61 m (2 ft).

(2) Straight Deep Drop (Scenario 2; Away from the pedestal)

The dropping mass impacts the rack baseplate. It shall be demonstrated that the baseplate is not pierced, and the pool liner does not sustain a direct impact. For the postulated deep drop event (away from the pedestal), the deformed baseplate of the rack must not impact the pool liner. The distance between the baseplate and the pool liner is 210 mm (8.27 in) and 185 mm (7.28 in) for new and spent fuel storage racks, respectively.

(3) Straight Deep Drop (Scenario 3; Over a pedestal)

For the postulated deep drop event (over a pedestal), the compressive stress on the concrete floor underneath the embedment plates shall not be exceeded the maximum allowable stress of 16.4 MPa (2,375 psi) as specified on the paragraph 5.3.4.4 of design specification (Reference 12).

(4) Stuck Fuel Assembly (Scenario 4)

Similar to the shallow drop accident, the damage of the cell wall shall be limited to the portion of the cell above the top of the "poison zone". The distance measured from the top of the rack to the upper boundary of the "poison zone" is 0.61 m (2 ft).

4.3 Analysis Method

The rack structure must either absorb the energy elastically or sustain some degree of plastic deformation. If the rack behaves plastically, the energy dissipated by plastic deformation is assumed equal to the kinetic energy of the impact. Based on this assumption, the extent of the damage to the upper portion of the cell structure or, in the case of a deep drop, to the rack base structure can be determined. This calculation covers the new fuel storage racks in NFP and the spent fuel storage racks of Region I and Region II in SFP. Region I racks are structurally stronger than Region II racks. To conservatively estimate the damage of the racks due to the postulated drop accidents, the calculation is performed for Region II racks. Since the new fuel storage rack is held down by firmly attached to the embedment plates of NFP using a stud bolt and is supported by additional intermediate plate, and has no “poison zone”, the drop accident evaluation is performed only for the case of drop (away from pedestal) on baseplate of the fuel rack.

4.3.1 Calculation of Impact Velocity

The objective of the analysis is to calculate the final velocity of the dropping object. A dropping object is modeled as a single lumped mass under the influence of gravity in a drag inducing medium. The effects of buoyant mass, gravity, and fluid drag are accounted for in the model. The drag force is based on the exposed frontal area of the fuel assembly. The governing equation to calculate the impact velocity for a body of mass subject to gravity and drag effects is

$$\left(M + M_V\right)\cdot\frac{dv}{dt} + \frac{C_D}{2}\cdot\rho_w\cdot A_D\cdot v^2 = \left(M - M_V\right)\cdot g \qquad (4\text{-}1)$$

where,

M : Mass of dropping object (fuel assembly along with the handling tool),
M_V : Buoyant mass of dropping object,
C_D : Drag coefficient,
ρ_w : Density of the water,
A_D : Area for drag force,
v : Velocity of dropping object, and
g : Acceleration of gravity.

The above nonlinear second order differential equation is solved to obtain the impact velocity of dropping object as shown below:

With $\varepsilon = M_V / M$, Equation (4-1) is

TS

[redacted]

4.3.2 Methodology for Straight Shallow Drop Accident

The straight shallow drop accident analysis determines the extent of the damage to the rack structure due to the impact of dropping object. The impact velocity of the dropping mass is calculated first to determine the bounding kinetic energy that will be used later for the damage evaluation due to the postulated shallow drop accident. If the impact occurs on a single edge of one storage cell, then the load will shift to the corners of the cell. The impact load should then cause a number of adjacent cell walls to be crushed.

The ultimate load carrying capacity of a single wall is calculated using an empirical formula in theory of elastic stability (Reference 17). Once the ultimate load, P_{ult}, is reached in a cell wall, large deformation occurs until the work done by P_{ult} equals the impact energy. Therefore, the energy balance equation can be described as follows:

$$1/2 \times \text{Dropping Mass} \times \text{Velocity}^2 = (N_{walls} \times P_{ult} - \text{Buoyant Weight}) \times \text{Crushed Distance}$$

where,

N_{walls} : Number of cell walls crushed, and
P_{ult} : Ultimate load carrying capacity in the cell wall.

The ultimate load carrying capacity is given as $P_{ult} = C \times t_{cell}^2 \times (E \times S_y)^{0.5}$, where C is a factor which depends on the cell thickness (t_{cell}) to cell width ratio and on the ratio E / S_y. The cited reference contains a curve from which C is determined.

4.3.3 Methodology for Straight Deep Drop Accident (Away from the Pedestal)

When a dropping object impacts to the baseplate of a rack, the deformation of the baseplate and the potential for impact on the pool liner is evaluated.

The energy dissipated by plastic deformation of the baseplate is calculated as

TS

4.3.4 Methodology for Straight Deep Drop Accident (Over a Pedestal)

The velocity of the dropping object just prior to impact with the rack baseplate is calculated using the equation (4-3) as stated on subsection 4.3.1. The stress wave in the pedestal will propagate at the fastest speed if the drop occurs in the lightest rack because the post-impact velocity of the rack is the greatest in this rack. Conservation of momentum predicts that the post-impact velocity (V) is calculated as follows:

$$V = \frac{W}{W + W_{rack}} \cdot v_f$$

where,

W : Weight of dropping object (fuel assembly along with the handling tool),
W_{rack} : Weight of spent fuel rack (empty), and
V_f : Velocity of the dropping object just prior to impact with the rack baseplate.

By assuming the pedestal acts like a bar, the stress in the pedestal (S) is calculated by the post-impact velocity of the rack using the following equation:

$$S = \sqrt{E \cdot \frac{\gamma}{g}} \cdot V$$

where,

E : Young's modulus of pedestal material, and
γ : Weight density of pedestal material.

The force transmitted to the pool slab is calculated by multiplying the stress in the pedestal and the area of male pedestal diameter together. This transmitted load will be worked on a concrete slab through the embedment plate under the pedestal of racks. As a result, the compressive stress on concrete due to dropping mass is calculated considering the embedment plate size and compared with the allowable stress limit specified on section 4.2.

4.3.5 Methodology for Stuck Fuel Accident

This is the evaluation for the ability of the rack walls to withstand the uplift force on a stuck fuel assembly. There are a number of ways that a fuel assembly can become stuck in a cell. Three most limiting cases are considered for the uplift force evaluation. A classical strength of materials equation is used to determine the amount of area needed to support the uplift force on a stuck fuel assembly.

(1) Vertical uplift force at top of cell

The critical location for load application is to have this load applied near the top of the rack along or against a single cell wall. If the vertical uplift load is resisted only by shear stress and the allowable in shear is the Level B limit. The depth (h_{sf}) of the cell that can support the applied load is obtained from the classical strength of materials equation to determine the amount of area needed to support the forces. If the damage depth of the cell is above the active fuel area, the vertical uplift force is not a safety concern.

$$h_{sf} = \frac{F_{Uplift}}{2 \cdot \tau_y \cdot t_{cell}}$$

where,

F_{Uplift} : Uplift force applied to the rack,

τ_y : Allowable in shear of cell wall for Level B limit (=1.33 x 0.4 x S_y), and

t_{cell} : Cell wall thickness.

(2) Vertical uplift along length of cell

The cell wall stress (σ) due to vertical uplift force along length of cell is determined as follows:

$$\sigma = \frac{F_{Uplift}}{D_{cell} \cdot t_{cell}}$$

where,

D_{cell} : Cell Inside dimension.

If the calculated stress using above equation is below the yield strength of rack cell, the permanent damage of the cell will not occur.

(3) Horizontal and vertical force (45 degree inclined force)

If the load is applied inclined at 45 degrees, then there is a horizontal load that must be supported. Realistically, this load can only be applied at the top of the rack. Therefore, any damage is confined to a region above the active fuel area. The depth (h_{sf}) of the damaged region is obtained from the following equation to determine the amount of area needed to support the forces.

$$h_{sf} = \frac{F_{Uplift}}{2 \cdot \sqrt{2} \cdot \tau_y \cdot t_{cell}}$$

The damaged region by tear out of a cell wall shall be less than the distance from the rack top to the edge of the neutron absorber material.

4.4 Assumptions

(1) The trajectory of the dropped objects is vertical, which minimizes the fluid drag. This assumption increases the impact velocity and results in higher energy impacts.

(2) The ultimate load that can be sustained by a cell wall is based on the load carrying capacity of thin plate sections.

(3) The energy absorbed through failure of connecting welds is ignored in the analysis.

4.5 Results of Analyses

The postulated drop accidents analyses are conservatively performed based on the bounding impact energy and configuration. The impact velocities for mechanical accident scenarios 1, 2 and 3 are summarized in Table 4-1. The following results are determined based on the methodologies, which are discussed on section 4.3, and the detailed calculations are described in the mechanical accident analysis report (Reference 18).

(1) Straight Shallow Drop (Scenario 1)

In the straight shallow drop of a fuel assembly along with the handling tool, it is demonstrated that the permanent damage to any fuel storage cell is limited to the maximum depth of 64.3 mm (2.53 in) below the top of the rack. This is less than the distance from the top of the rack to the beginning of the active fuel region, 0.61 m (2 ft). Therefore, there will be no effect on the configuration and subcriticality of the fuel in the adjacent cells due to this accident.

(2) Straight Deep Drop (Scenario 2)

During a straight deep drop accident away from the pedestal locations, the baseplates of the new and the spent fuel storage racks do not experience gross failure (puncture) because the deformed depth of the baseplate is smaller than the baseplate thickness of 25 mm (0.984 in). Furthermore, the deformation amounts of the baseplates of the new and the spent fuel storage racks are calculated as 138.9 mm (5.47 in) and 117.1 mm (4.61 in), respectively. These values are less than the minimum distances between the baseplate and the liner, which are 210 mm (8.27 in) and 185 mm (7.28 in) for the new and the spent fuel storage racks, respectively. Therefore, a dropped fuel assembly along with the handling tool will not cause the result that the rack baseplate impacts the pool liner.

(3) Straight Deep Drop (Scenario 3)

In the straight deep drop accident over a pedestal, the resulting impact transmits a load of 31,877 kgf (70,276 lbf) to the concrete pool slab through the embedment plate under the pedestal of racks. The compressive stress due to this impact load on concrete pool slab is calculated as 4.0 MPa (581 psi) by using a classical strength of materials equation, which is less than allowable stress limit of 16.4 MPa (2,375 psi). Therefore, the compressive stress on concrete due to dropping mass is less than the allowable stress limit.

(4) Stuck Fuel Assembly (Scenario 4)

The fuel racks are adequate to withstand the uplift force of 2,268 kgf (5,000 lbf) due to a stuck fuel assembly. The maximum depth of the damaged cell wall for the vertical uplift force at top of cell is found to be limited to within 56.9 mm (2.24 in) below the top of the rack. The damaged region by tear out of a cell wall for the 45 degrees inclined force would occur within the 40.1 mm (1.58 in) of the cell length. These are less than the distance from the top of the rack to the beginning of the active fuel region, 0.61 m (2 ft). In addition, the cell wall stress due to vertical uplift force along length of cell of 36.9 MPa (5,354 psi) is less than the yield strength of 78.5 MPa (21,400 psi). Therefore, the stuck fuel accident analysis demonstrates that the damage of the cell wall would only occur above the neutron absorber and the permanent deformation of cell does not occur.

Table 4-1 Impact Evaluation Data

Rack	Cases	Drop Weight(*), kgf (lbf)	Drop Height, m (in)	Impact Velocity, m/sec (in/sec)
NFSR	Straight Deep Drop (Away from Pedestal)	1,100 (2,425)	5.18 (203.9)	10.1 (396.8)
SFSR	Straight Shallow Drop	1,100 (2,425)	0.61 (24.0)	3.14 (123.6)
	Straight Deep Drop (Away from Pedestal)	1,100 (2,425)	5.2 (204.7)	7.68 (320.2)
	Straight Deep Drop (Over a Pedestal)	1,100 (2,425)	5.2 (204.7)	7.18 (282.6)

(*) Drop Weight = Fuel assembly along with the handling pool

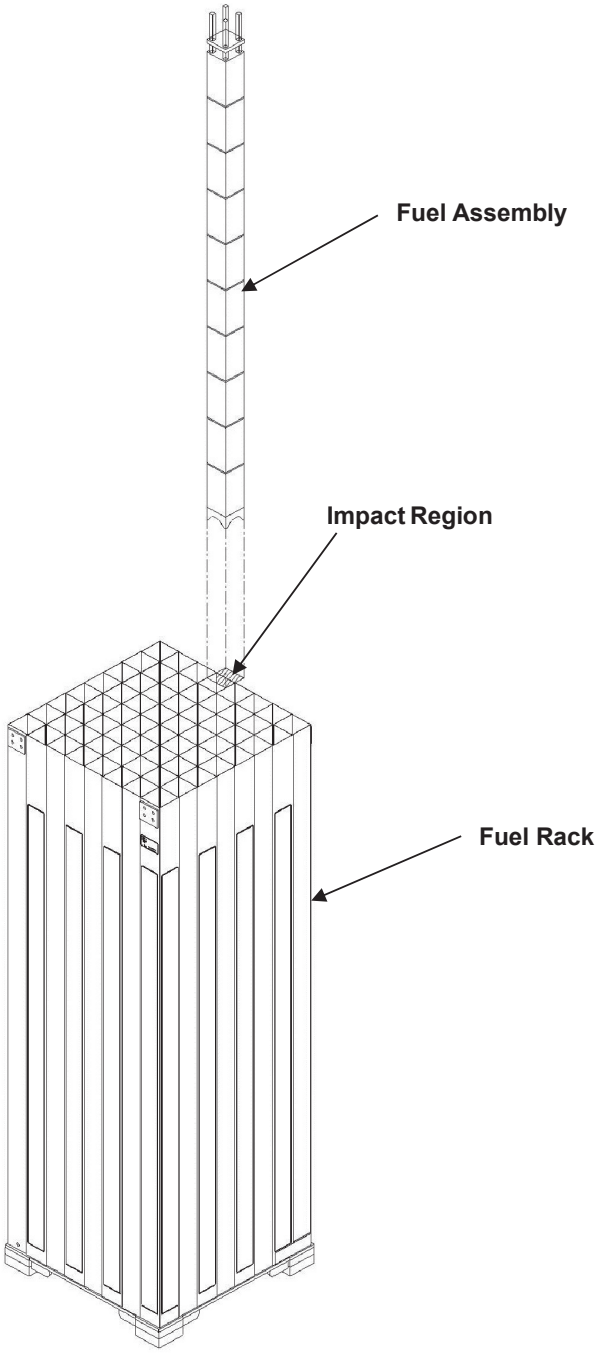

Figure 4-1 Schematic of the Straight Shallow Drop

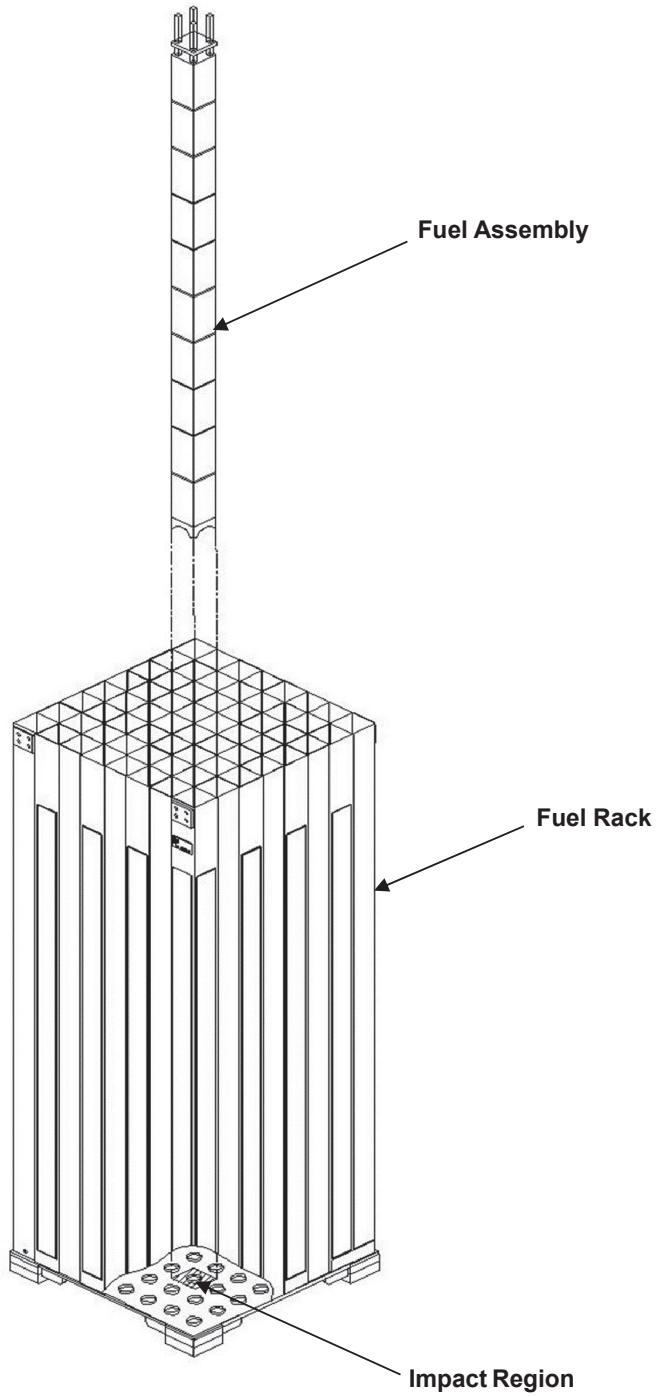

Figure 4-2 Schematic of the Deep Drop Scenario-1

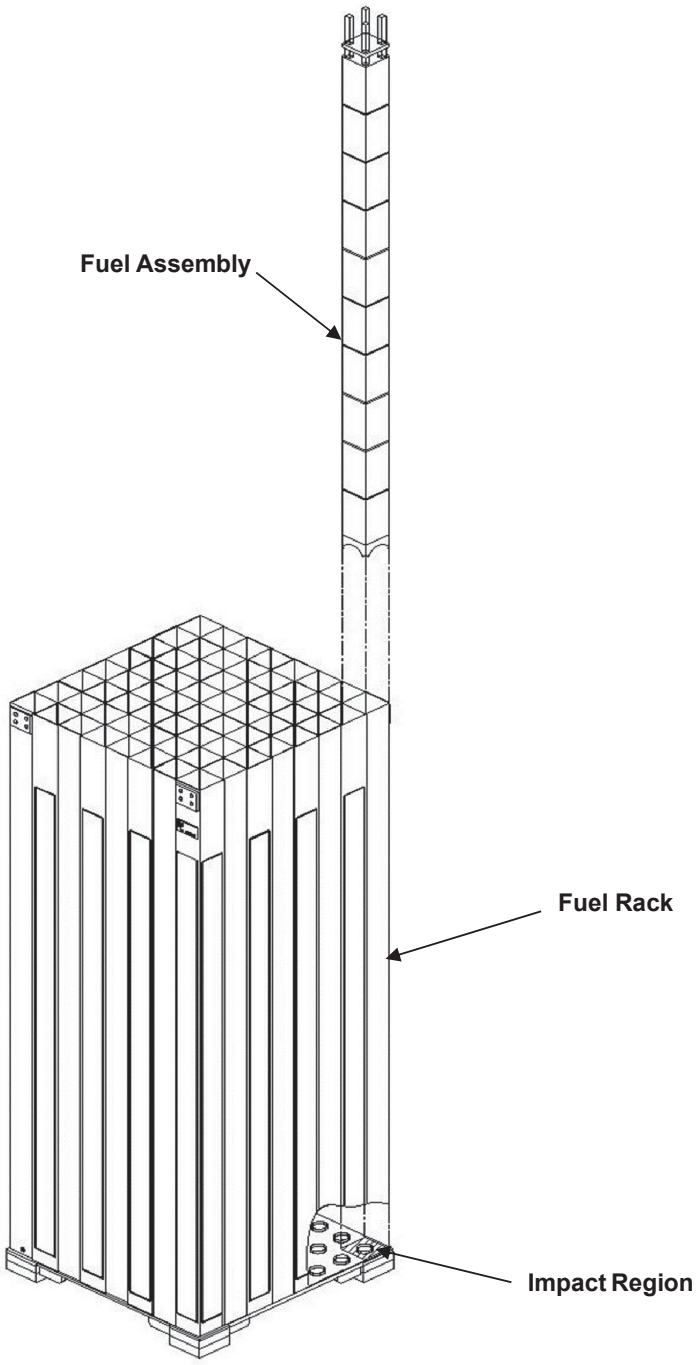

Figure 4-3 Schematic of the Deep Drop Scenario-2

5 CONCLUSIONS

The design of the new and spent fuel storage racks of the APR1400 design is acceptable because the results of structural and seismic analyses and mechanical accident analyses meet all requirements. The results are summarized as follows:

(1) There is no impact on the rack-to-pool wall and on the rack cell-to-cell.

(2) The overturning of rack module under seismic events does not occur.

(3) The SFSRs does experience the impact on rack-to-rack during SSE events at the baseplate because they are installed in contacts with adjacent baseplate of other racks. However, the calculated impact loads are lesser than the capacity limit of the baseplate.

(4) All rack cell wall and pedestal stress factors are below the allowable stress factor limit.

(5) All weld stresses are below the allowable stress limits.

(6) The fuel spacer grid does not buckle and the bending stress induced in the fuel rod cladding is well below the yield strength of the fuel rod clad. Therefore, the structural integrity of the spent fuel assembly is maintained.

(7) The NFSRs and the SFSRs under the postulated mechanical accident possess acceptable margins of safety.

(8) A stuck fuel assembly does not cause a bounding stress condition.

Therefore, it is demonstrated that the design of the NFSRs and the SFSRs of the APR1400 design meets the structural integrity requirements for Level A and Level D conditions which are specified on NRC SRP 3.8.4, appendix D (Reference 1).

6 REFERENCES

1. NUREG-0800, Standard Review Plan, Section 3.8.4, “Other Seismic Category I Structures,” Rev. 4, U.S. Nuclear Regulatory Commission, September 2013.

2. NUREG-0800, Standard Review Plan, Section 3.7.1, “Seismic Design Parameters,” Rev. 3, U.S. Nuclear Regulatory Commission, March 2007.

3. Rabinowicz, E., “Friction Coefficients of Water Lubricated Stainless Steels for a Spent Fuel Rack Facility,” MIT, Report for Boston Edison Company, 1976.

4. S. Singh, et. Al., “Structural Evaluation of Onsite Spent Fuel Storage: Recent Developments,” Proceedings of the Third Symposium, Orlando, Florida, December 1990, North Carolina State University, Raleigh, NC 27695, pp V/4-1 through V/4-18.

5. Fritz, R.J., “The Effects of Liquids on the Dynamic Motions of Immersed Solids,” Journal of Engineering for Industry, Trans. of ASME, February 1972, pp 167-172.

6. Computer code, ANSYS Version 10.0; Installed on HP Integrity Superdome 16 Way of Hewlett Packard Co., Verification Document No. DAVM100, Rev.0, July 2006.

7. Structural and Seismic Analysis Report for New and Spent Fuel Storage Racks, N14014-224CN-0001, Rev.0, December 2014. (Doosan Proprietary)

8. ASME Boiler and Pressure Vessel Code, Section III, Division 1, “Rules for Construction of Nuclear Facility Components,” The American Society of Mechanical Engineers, the 2007 Edition with the 2008 Addenda.

9. NUREG-0800, Standard Review Plan, Section 3.8.5, “Foundations,” Rev. 4, U.S. Nuclear Regulatory Commission, September 2013.

10. Outline Drawing, N13027-224CD-1000, “New Fuel Storage Pit Layout,” Rev.1, November 2014. (Doosan Proprietary)

11. Outline Drawing, N13027-224CD-2000, “Spent Fuel Pool Layout,” Rev.1, November 2014. (Doosan Proprietary)

12. KEPCO Engineering & Construction Co. Inc., KEPCO E&C Job No. 11E47, 1-423-N462-003, "Design Specification for Fuel Storage Rack," Revision 0, December 2014.

13. Regulatory Guide 1.61, “Damping Values for Seismic Design of Nuclear Power Plants,” Rev. 1, U.S. Nuclear Regulatory Commission, March 2007.

14. ASME Boiler and Pressure Vessel Code, Section II, “Materials,” The American Society of Mechanical Engineers, the 2007 Edition with the 2008 Addenda.

15. SANDIA Report, SAND90-2406, “A Method for Determining the Spent-Fuel Contribution to Transport Cask Containment Requirements,” Sandia National Laboratories, November 1992.

16. Timoshenko, S.P., “Strength of Materials,” 3rd Edition, Part II.

17. Timoshenko & Gere, “Theory of Elastic Stability,” McGraw-Hill, 1961.

18. Accident Analysis Report for New and Spent Fuel Storage Racks, N14014-224CN-0002, Rev.0,

December 2014. (Doosan Proprietary)